Shelf-derived mass-transport deposits: origin and significance in the stratigraphic development of trench-slope basins

Barbara Claussmann, Julien Bailleul, Frank Chanier, Geoffroy Mahieux, Vincent Caron, Adam D. Mcarthur, Corentin Chaptal, Hugh E. G. Morgans, Bruno C. Vendeville

Shelf-derived mass-transport deposits: origin and significance in the stratigraphic development of trench-slope basins

Claussmann B.[1,2,*], Bailleul J.[1], Chanier F.[3], Mahieux G.[4], Caron V.[4], McArthur A. D.[5], Chaptal C.[1], Morgans H. E. G. [6], Vendeville B. C.[3]

1. U2R 7511, Basins-Reservoirs-Resources (B2R), Geosciences department, UniLaSalle - University of Picardie Jules Verne, 60026, Beauvais, France
2. Schlumberger, Software Integrated Solutions, London, SW1E 6AJ, United Kingdom
3. University of Lille, CNRS, ULCO, UMR 8187, Laboratory of Oceanology and Geosciences (LOG), Lille, France
4. U2R 7511, Basins-Reservoirs-Resources (B2R), University of Picardie Jules Verne - UniLaSalle, 80039 Amiens, France
5. School of Earth and Environment, University of Leeds, Leeds, LS2 9JT, United Kingdom
6. GNS Science, Lower Hutt, New Zealand

Accepted Manuscript version (unedited PDF accepted for publication).

Published Journal Article version available online, 27 May 2021:
https://www.tandfonline.com/doi/abs/10.1080/00288306.2021.1918729?journalCode=tnzg20

Published by Taylor & Francis in the New Zealand Journal of Geology and Geophysics, Special issue: Sedimentary systems of the Hikurangi Subduction Margin.

*Correspondence: bclaussmann@slb.com

1. ABSTRACT

Continental shelves generally supply large-scale mass-wasting events. Yet, the origin and significance of shelf-derived mass-transport deposits (MTDs) for the tectonostratigraphic evolution of subduction complexes and their trench-slope basins have not been extensively studied. Here, we present high-resolution, outcrop-scale insights on both the nature of the reworked sediments, and their mechanisms of development and emplacement along tectonically active margins, by examining the Middle Miocene shelf-derived MTDs outcropping in the exhumed southern portion of the Hikurangi subduction margin. Results show that periods of repeated tectonic activity (thrust propagation, uplift) in such compressional settings not only affect and control the development of shelfal environments but also drive the recurrent generation and destruction of oversteepened slopes, which in turn, favour the destabilisation and collapses of the shelves and their substratum. Here, these events produced both large-scale, shelf-derived sediment mass-failures and local debris flows, which eventually broke down into a series of coalescing, erosive, genetically-linked surging flows downslope. The associated MTDs have a regional footprint, being deposited across several trench-slope basins. Recognition of tectonic activity as another causal mechanism for large-scale shelf failure (in addition to sea-level changes, high-sedimentation fluxes) has implications for both stratigraphic predictions and understanding the tectonostratigraphic evolution of deep-marine fold-and-thrust belts.

Keywords: active margin, shelf failure, intra-slope basins, mass-wasting deposits, outcrop study, tectonics

2. INTRODUCTION

Along active margins, tectonics predominate and exert a crucial control on the stratigraphic development of the related sedimentary basins (*e.g.,* trench-slope basins) and their basin-bounding structures (Moore and Karig 1976; Karig et al. 1980; Underwood and Bachman 1982; Chanier and Ferrière 1991; Underwood and Moore 1995; Bailleul et al. 2013; McArthur et al. 2019). Recurrent mass-wasting occurs and thus, associated mass-wasting products, known as mass-transport deposits (MTDs) form throughout the margin's history, flanking the sedimentary basins, such as trench-slope basins (Moore and Karig 1976; Underwood and Bachman 1982; Bailleul et al. 2007; Vinnels et al. 2010; Festa et al. 2015; Ortiz-Karpf et al. 2018; McArthur et al. 2019).

A diverse range of MTDs has been described along tectonically active margins (Moscardelli and Wood 2015; Festa et al. 2016 and references therein) and numerous studies have investigated the potential causal mechanisms for the related mass-wasting events (*e.g.,* Pickering & Corregidor 2005; Moscardelli et al. 2006; Lamarche et al. 2008; Romero-Otero et al. 2010; Vinnels et al. 2010; Gamberi et al. 2011; Nelson et al. 2011; Strasser et al. 2011; Urgeles & Camerlenghi 2013; Ogata et al. 2014; Alves 2015; Lehu et al. 2015; Festa et al. 2016; Ortiz-Karpf et al. 2018; Festa et al. 2019; Moore et al. 2019; Ogata et al. 2019; Raymond 2019; Carey et al. 2019).

Based on the relationships that exist between their source region, sizes, and potential causal mechanisms, Moscardelli and Wood (2008) and Moscardelli and Wood (2015) proposed to refine the classification of mass-wasting products by grouping them into *attached* and *detached* systems, respectively (1) sourced from regional (*e.g.,* shelf) or local slopes; (2) regionally extensive (potentially reaching hundreds to thousands of square kilometres in area, tens of kilometres in width and length, and hundreds of metres in thickness) or smaller, local (occupying less than tens of square kilometres in area and a few kilometres in width and length); and (3) essentially controlled by extrabasinal regional processes (*e.g.,* climate) or localised gravitational instabilities (Figure 1).

Continental shelves unequivocally supply some of the greatest mass-wasting events and deposits recorded worldwide (*i.e., attached* systems) (Posamentier and Walker 2006). Yet, the origin and significance of shelf-derived mass-wasting products for the tectonostratigraphic evolution of subduction complexes and their related trench-slope basins have not been extensively scrutinised.

In this study, we propose to address this knowledge gap by presenting new occurrences of mass-wasting systems, sourced from the shelf, cropping out in the emerged southern portion of the Hikurangi

subduction wedge (Coastal Ranges, North Island of New Zealand) (Figure 2). The related products are Middle Miocene in age and include several episodes of mass-wasting that reworked shelf-derived material (macrofaunas and sediments), can reach over 100 metres (minimum thickness, not decompacted) at outcrop and were deposited across several trench-slope basins along a 70 kilometre-long transect (Whareama, Te Wharau and Akitio trench-slope basins) (Figure 3).

Most studies on the shelf-derived mass-wasting events and deposits are based on seismic-reflection data. Therefore, this work aims at bringing new high-resolution, outcrop-scale insights on both the nature of the reworked sediments, and the mechanisms of development and emplacement of these MTDs along tectonically active margins. Sea-level changes and high sedimentation rates are commonly inferred to be the main causal mechanisms triggering the large-scale destabilisation, downslope mass-transport and resulting deposition of shelf-derived sediments into deep-water (Posamentier and Kolla 2003; Moscardelli and Wood 2008; Moscardelli and Wood 2015; Bull et al. 2020). Yet, the role of tectonics is undoubtedly important, particularly along active margins (*e.g.,* Lewis et al. 2004; Lamarche et al. 2008; Watson et al. 2020; Couvin et al. 2020).

Here, we specifically explore how continued period of tectonic activity (shortening, uplift and related seismicity) can lead to the recurrent generation and destruction of oversteepened slopes at the shelf-margins and in turn favour the repeated destabilisation and collapses of the shelf(ves).

Specific objectives are to:

- Describe the nature, geometries and internal characteristics of the reworked sediments (*e.g.,* lithofacies) and assess the implication for subsurface assessment of similar, seismic-scale MTDs,
- Gain a better understanding on the mechanism of development and emplacement of shelf-derived MTDs in subduction complexes,
- Use the lithofacies and their associations to reconstruct the depositional environments and palaeogeography of the Coastal Ranges of the Hikurangi Margin during the Middle Miocene,
- Highlight the role of shelf-derived MTDs as markers of the tectonic activity in mature trench-slope basins.

3. GEOLOGICAL SETTING

3.1. Geological history

The Hikurangi subduction wedge started to form about 25 Ma ago as a result of the westward subduction of the oceanic Pacific Plate beneath the Australian Plate along the eastern margin of the North Island of New Zealand (Figure 2) (Ballance 1976; Spörli 1980; Pettinga 1982; Chanier and Ferrière 1991; Field et al. 1997; Nicol et al. 2007).

Bounded by the Hikurangi Trench to the south-east and the Forearc Basin *sensu stricto* to the west, the Hikurangi subduction wedge is made of a series of elongate, trench-parallel intra-slope basins (*i.e.,* trench-slope basins (*sensu* Underwood and Moore 1995)) separated and confined by tectonically active, sublinear bathymetric highs that are controlled by underlying landward-dipping thrust faults and asymmetrical seaward-verging folds (Lewis and Pettinga 1993; Barnes et al. 2010; Bailleul et al. 2013; Bland et al. 2015; McArthur et al. 2019).

Since the onset of subduction, the Hikurangi subduction wedge has undergone a complex and polyphased tectonic history (Figure 4).

As the Pacific Plate began to subduct beneath the Australian Plate, the related compressional stresses resulted in the seaward emplacement of ESE thrust nappes (25 – 18 Ma), on the back of which thrust-bounded depocenters provided the necessary space for the development of trench-slope basins (17.5 – 15 Ma) (Pettinga 1982; Chanier and Ferrière 1989; Chanier and Ferrière 1991; Rait et al. 1991; Nicol et al. 2007; Bailleul et al. 2013; Malie et al. 2017).

Then, from Middle to Late Miocene times (15 – 6.5 Ma), the entire margin experienced a period of mixed N-S to NE-SW extension and compression, leading to general subsidence, gravitational collapses and normal faulting in the inner portion of the wedge, as well as continued outward migration of the deformation front in the middle and outer portions (Chanier 1991; Chanier et al. 1999; Barnes et al. 2002; Bailleul et al. 2013).

Finally, from the Late Miocene to present-day (6.5 – 0 Ma), renewed E-W to NW-SE compressional deformation and tectonic inversion dominated the margin and resulted in regional folding and reverse faulting. Shortening has accelerated within the last million year and has led to the uplift and emergence of part of the inner portion of the subduction wedge (*i.e.,* trench-slope break), which now forms the Coastal Ranges of the eastern North Island of New Zealand (Figure 2) (Lamb and Vella 1987; Cape et al. 1990;

Chanier 1991; Chanier et al. 1999; Nicol et al. 2002; Nicol et al. 2007; Bailleul et al. 2013) and outboard frontal accretion (Barnes et al. 2018).

The close interplay between the evolution of the margin and the development of the associated sedimentary basins resulted in intricate trench-slope basin fills that are disrupted by a series of discontinuities (Neef 1992; Neef 1999; Bailleul et al. 2007; Bailleul et al. 2013; Burgreen and Graham 2014; McArthur et al. 2019).

Their fills mostly comprise Miocene to Recent deep-marine gravity-driven deposits, extensive marine hemipelagic mudstones and carbonate deposits (Figure 4) (Field et al. 1997; Lee and Begg 2002; Bailleul et al. 2007; Bland et al. 2015; McArthur et al. 2019). They conformably or unconformably overlie the Cretaceous to Paleogene pre-subduction basement, which can be divided into two main assemblages: (1) the Lower Cretaceous Torlesse greywackes, witness of an older accretionary prism developed along the south-eastern margin of Gondwana at the time (Spörli 1980; Bradshaw 1989; Mortimer 2004); and (2) the Upper Cretaceous to Oligocene series evolving from detrital to pelagic sediments eastward (Figure 4) (Chanier and Ferrière 1991) and indicating a sustained period of tectonic quiescence (Chanier 1991; Chanier and Ferrière 1991; Bailleul et al. 2013).

3.2. Whareama and Te Wharau Basins

The study area is located in the southern Coastal Ranges, and more particularly in the exhumed Whareama and Te Wharau Basins (Figure 3; Figure 5).

The Whareama Basin is an elongate, NE-SW trench-parallel slope basin (Figure 3), ~50 kilometres long and two to six kilometres wide, bounded by basement ridges composed of pre-Miocene strata (Chanier 1991). It started to form contemporaneously with the onset of subduction on the backlimb of the Glenburn Nappe, a seaward-verging thrust nappe (Chanier 1991; Chanier and Ferrière 1991) that is composed of Lower Cretaceous Torlesse greywackes and Upper Cretaceous to Eocene pelagic to detrital series (Figure 4; Figure 5). Its sedimentary fill unconformably to conformably overlies the Glenburn Nappe and is bounded to the west by the Adams-Tinui Fault complex and Pukeroro Fault (*i.e.,* landward basin margins, Figure 3; Figure 5) and to the east by the Flat Point-Whakataki Fault complex (*i.e.,* seaward basin margin, Figure 3; Figure 5).

The Te Wharau Basin is another elongate, thrust-bounded slope basin located in the emerged, inner-portion of the subduction wedge (Figure 3). To the west of the Whareama Basin, the Te Wharau Basin is smaller (~10 kilometres long), narrower (one to five kilometres wide) and oriented North-South (Figure 3;

158 Figure 5) (Chanier 1991; Bailleul et al. 2013). Its fill unconformably overlies the Lower Cretaceous
159 Torlesse greywackes (to the north) as well as the Upper Cretaceous to Eocene detrital series (to the
160 south) (Chanier 1991) (Figure 4; Figure 5). The Adams-Tinui Fault complex represents its seaward basin
161 margin (Figure 3), except in the central portion of the system, where it comprises two synclines and is
162 bounded by both the Adams-Tinui Fault complex and the Pukeroro Fault (Figure 5). Unlike the Whareama
163 Basin, the Te Wharau Basin only records deposits from the Middle to Upper Miocene (Chanier 1991).

164 ### 3.3. Depositional systems

165 Gravity-driven deposits dominate the stratigraphic infill of trench-slope basins (Underwood and Bachman
166 1982; Underwood and Moore 1995; Underwood et al. 2003; Vinnels et al. 2010). Although submarine
167 canyons and channels play an undeniable role in the distribution of sediments, slope destabilisation can
168 act as another, agent of sediment delivery and reorganisation, triggering significant submarine mass-
169 failure and reworking (Underwood and Bachman 1982; Chanier and Ferrière 1991; Bailleul et al. 2007;
170 McArthur et al. 2019; McArthur and McCaffrey 2019).

171 In this study, we specifically focus on the Middle Miocene, Lillburnian (Late Langhian to Serravallian, 15.1
172 – 13.05 Ma) mass-wasting events that reworked shelf-derived material. The related mass-wasting
173 products crop out in the preserved portions of the Whareama and Te Wharau Basins, as well as in the
174 Akitio Basin farther north (Figure 3, sections b, c, n, r, s, tw).

175 Even though deep marine sedimentation dominated at the time, several contemporaneously developing
176 and older (Figure 4) shallow-marine, mixed siliciclastic-carbonate shelves were also reported in the area
177 (Figure 3, sections f, i, m, ms, o, p, t, w) (Crundwell 1987; Chanier 1991; Bailleul et al. 2007; Bailleul et
178 al. 2013; Caron et al. 2019; Bailleul et al. Submitted; Caron et al. 2021). Bailleul et al. (2013) and Bailleul
179 et al. (Submitted) demonstrated that whether attached to the continent or not, these shelfal systems
180 preferentially formed above trench-slope basin-bounding structures that were affected by active-margin
181 tectonic activity, such as uplift events. The abrupt shallowing provided the suitable depositional settings
182 (*e.g.,* neritic conditions) for carbonates and biogenic sediments.

183 ## 4. DATA AND METHODS

184 We undertook fieldwork in order to characterise the Middle Miocene strata outcropping in the southern
185 emerged portion of the Hikurangi subduction wedge. Over one kilometre of sea cliff outcrop along the
186 Whareama Basin coastline was mapped and studied through acquisition of photogrammetric data

(acquired from a drone), traditional fieldwork data (*e.g.,* detailed sedimentary sections) and taphonomic data (Figure 5, Sefton Hills outcrops, sections s-1 and s-2). In parallel, several hinterland localities were also characterised through a series of outcrop observations in the Te Wharau Basin (Figure 5, sections c, n, r, tw-1, tw-2). In the Akitio Basin, the contemporaneous MTD occurrences (Figure 3, section b) were previously described by Bailleul et al. (2007) and Bailleul et al. (2013).

4.1. Drone acquisition and photogrammetry

Ground Control Point (GCP) coordinates and drone pictures of the one-kilometre-long coastal outcrop at Sefton Hills were acquired so that a 3D georeferenced model could be built to observe and describe the lateral and vertical variations of the sediment distribution. Over 500 high-resolution aerial images were captured with a DJI Phantom 4 Pro UAV, and a total of nine GCP coordinates were recorded using a Trimble GeoExplorer 2008 differential global positioning system tool (DGPS) as well as a Trimble Tempest antenna positioned at two metres above the measured point. Standard *Structure from Motion* workflows (Westoby et al, 2012) were then followed for data quality control, processing and rendering. A 3D outcrop model was created in the form of a high-resolution triangulated mesh textured with the photographs using the Metashape Professional Edition software by Agisoft (Figure 6).

4.2. Geological mapping and outcrop sedimentology

Field mapping data were recorded with a Trimble ® TDC100 and integrated using ArcGIS software tools. The stratigraphic expressions of the Middle Miocene, Lillburnian aged gravity-driven deposits were examined along the coast at Sefton Hills and captured in three detailed sedimentary sections (total of 165 metres at bed scale, Figure 7). Detailed structural measurements (*e.g.,* ductile deformation analysis), as well as bedding and palaeocurrents were also collected. These measurements were corrected using the geomagnetic models from GNS Science New Zealand. A dedicated diagnostic feature template was used to thoroughly describe each MTD occurrence in a standardised manner, both along the coastline and in the hinterland. The age of the sedimentary units and the palaeobathymetries were defined using micro- and macropalaeontological analysis conducted by GNS Science New Zealand. Four samples were collected in the study area to supplement the information already captured in the Fossil Record Electronic Database (https://fred.org.nz/) (Appendix 1. Appendix 2).

4.3. Taphonomy

Due to the significant quantity of macrofossils contained in the MTDs, occurring both as whole skeletons and moderately fragmented remains, a taphonomic analysis was performed in three sectors of the Sefton Hills depositional system on approximately one square metre area of outcrop. It was restricted to the coarsest fraction of death assemblages contained in the MTDs, *i.e.,* on fossil remains larger than five millimetres allowing assignment to a taxonomic group (from, at best, Species to Class level). In this study, three categories of skeleton damage, namely fragmentation, abrasion and bioerosion, were described visually using the graded classification scale presented in Appendix 3, complemented by those proposed by Caron (2011) and Caron et al. (2019). Encrustation of skeletons was also evaluated but was found to be virtually absent. This approach aims at (1) extending the sedimentological knowledge on transport and depositional processes in gravity-driven systems, (2) helping better characterise the source areas and (3) defining diagnostic characteristics to help distinguish between MTDs.

4.4. Lithofacies, facies associations and depositional environments

The integration of the detailed fieldwork with the digital outcrop model (Figure 6; Figure 7) enabled us to document the lateral and vertical facies variations, recognise the stratigraphic architectures and thus propose facies assemblages and associated depositional environments (Table 1; Figure 8; Figure 9; Figure 10; Figure 11). The facies associations and interpretations follow and complement the initial nomenclature for trench-slope basins that was defined by Bailleul et al. (2007) and Bailleul et al. (2013), whereby **Fa1** refers to turbidite systems and **Fa3** to mass-wasting systems.

Because our study focuses on shelf-derived MTDs, we do not provide an extensive description of the turbidite lithofacies, already described in details along the margin (*e.g.,* Bailleul et al. 2007; Bailleul et al. 2013; Burgreen and Graham 2014; McArthur and McCaffrey 2019; McArthur et al. 2021), and we used the facies associations **Fa1g** and **Fa1s** defined by Bailleul et al. (2007) and Bailleul et al. (2013) as reference.

Alternatively, we scrutinised the different sedimentary expressions of the shelf-derived MTDs (**Fa3p**) recorded on outcrops and recognised four distinct lithofacies (**DF, MF-1, MF-2, SL)** (Table 1). The lithofacies comprise a variety of cohesive gravity flows (**DF, MF-1 and MF-2**) extensively observed and described in the Whareama and Te Wharau Basins (Figure 8, Figure 9, Figure 10; Figure 11) as well as chaotic and contorted facies (**SL**) only witnessed in the Akitio Basin (Bailleul et al. 2007; Bailleul et al.

2013). Altogether, the shelf-derived cohesive gravity flows form the facies assemblage **Fa3p-d** whereas the chaotic and contorted expressions form **Fa3p-s** (Table 1).

5. MIDDLE MIOCENE SHELF-DERIVED GRAVITY-DRIVEN SYSTEMS

5.1. Whareama Basin

In this study, we focus on a coastal transect from the eastern part of the Whareama Basin, at the Sefton Hills locality, which is situated four kilometres south of Uruti Point and can be divided into two sections, namely section s-1 and section s-2 (Figure 5). Section s-1 represents the main exposure that extends over one kilometre along the coast. Section s-2 is located 500 metres south of section s-1, on the beach (Figure 5). Both expose Middle Miocene, mid Lillburnian (Langhian, ca., 14 Ma) strata (Appendix 1).

Based upon the 3D outcrop model and detailed stratigraphic logging (Figure 6; Figure 7), two main gravity-driven systems and related deposits were identified. The contact between these two systems is stratigraphic, erosive yet can locally appear faulted on part of the outcrop.

5.1.1. Turbidite deposits

The lower part of the Sefton Hills outcrop (Figure 6) is characterised by a well-developed, several hundred metres thick turbidite system made of laterally continuous, mostly medium-bedded (average 17 centimetres thick), fine-grained sandstones. Shell fragments (either diffuse to abundant) and plant debris (either disseminated or organized) are frequent in the structured intervals, typically starting with coarse-grained sands. The overall net-to-gross is of ~65%; mud caps are thus common and on average 10 centimetres thick. They often present bioturbations such as *Phycosiphon* sp., *Chondrites* sp., *Zoophycos* sp. and *Thalassinoides* sp. Details on the lithology, stratification and internal bedding characteristics of the different sandstone intervals (**Fa1g** and **Fa1s** as defined by Bailleul et al. (2007) and Bailleul et al. (2013)) are given in Table 1.

Observations

Fa1g mostly comprises normally graded, amalgamated, slightly erosive, medium- to thick-bedded sandstones (Figure 6; Figure 8a, b, g, h). The thicker beds are made of (very) coarse- to fine-grained sands and their base, concave up, truncates the underlying strata with a low angle (centi- to decimetric scale incision). Channel-based drapes (*sensu* Barton et al. 2010) are not uncommon below the erosional

cut (Figure 8g, h). These turbidites sometimes evolve into several very fine- to medium-grained sandstone beds overlain by draping muddy layers, before alternating with either (1) fining and thinning upward interbedded sandstones and mudstones (**Fa1g-a**) (Figure 8a, b, g, h), or (2) finer and thinner interbedded mudstones and sandstones displaying local low-displacement features (**Fa1g-f**) (Figure 8b, c, d, e, f). The turbidites tend to be thicker (~20 centimetres), more massive and amalgamated at the top of the turbidite system (Figure 8d; Figure 9f), where they also include a couple episodes of concentrated bioclastic grits (10 to 20 centimetres thick) (Figure 7).

Most of the **Fa1g-f** occurrences are recorded in the lower part of the turbidite system, where they are often found interbedded with a series of tabular (sheet-like), continuous thin- to thick-bedded turbidites (**Fa1s**) (Figure 6; Figure 8e, f).

Palaeocurrent measurements were collected in the upper part of the system, along the sedimentary section SS-01 (Figure 7); they display a general SW-to-NE direction with a dispersion from the NW to the SE (Figure 6).

Interpretations

The facies association **Fa1s** was previously described by Bailleul et al. (2007) and Bailleul et al. (2013) and interpreted as sheet-like turbidites. These tabular, highly continuous turbidites commonly result from unconfined, waning turbidity currents (Lowe 1982; Kneller 1995) and either characterise the most distal region of a lobe setting before it evolves into basin plain environment (Galloway 1998) or the basin floor setting. These facies are generally associated with mixed to muddy systems which can disperse sand far into the basin (Galloway 1998). **Fa1s** is generally found interbedded with **Fa1g-f**, inferred to represent the lobe fringe facies from the medial to distal regions (Prélat et al. 2009; Burgreen and Graham 2014; McArthur et al. 2021). This interplay supports the presence of a particularly distal and unconfined setting at the start of the Sefton Hills system (**Fa1s**) that sometimes recorded the distalmost incursions (**Fa1g-f**) of a depositional lobe system.

The series then slowly evolve into more confined and proximal settings, recording the emplacement of a depositional lobe system, as was previously described and interpreted as **Fa1g** by Bailleul et al. (2007) and Bailleul et al. (2013) in the Akitio Basin. At Sefton Hills, **Fa1g** can be divided into **Fa1g-c**, **Fa1g-f** and **Fa1g-a** that have contrasting facies and internal architecture outlining the different parts of the lobe system.

Fa1g-c illustrates the network of small, low-relief distributary channel fills or scours (Galloway, 1998) that likely contributed to the development of the lobe system. **Fa1g-c** differs from lobe axis deposits usually

characterised by thick, amalgamated sandstone units and better compares to lobe off-axis deposits (Prélat et al. 2009; Burgreen and Graham 2014; McArthur et al. 2021). Although amalgamation is frequently observed, the strata is mostly medium-bedded and display a lower net-to-gross to the traditional lobe axis deposits (65% instead of 80%) (Prélat et al. 2009).

The small channel fills commonly show fining- and thinning- upward sequences (**Fa1g-a**) reflecting both the progressive abandonment of the distributary channel segment and filling of the unfilled relief (Galloway 1998; McHargue et al. 2011). The lobe fringe deposits (**Fa1g-f**) are less frequent towards the top of the sequence.

The nature (*e.g.,* shell fragments, plant remains) and abundance of debris in the deposit also highlight that the flow most likely initiated in a shallow marine environment that was continually connected to a hinterland sourcing the land-derived material (Kuenen 1964). Palaeocurrents recorded in the upper turbidite intervals indicate a sourcing from the WSW. Their variations (Figure 6) however outline that the flow of sediments occurred in fairly confined settings. Interactions between gravity currents and topography commonly result in spatial flow variations related to flow deflection (Kneller and McCaffrey 1999). We can thus infer the presence of a sublinear topography to the NE of the Sefton Hills locality, responsible for the deflection of the incoming turbidity currents. Yet, the presence of unconfined deposits (**Fa1s**) cropping out at the base of the Sefton Hills turbidite system suggest that such topography did not initially exist. It therefore developed coevally with the overriding **Fa1g** turbidite system.

5.1.2. Locally-derived mass-transport deposits

In the lower part of the Sefton Hills outcrop, the sandstone intervals are interspersed with recurrent, small-scale (one to five metres thick) chaotic, contorted (**Fa3l-s**) to matrix-supported (**Fa3l-d**) deposits (Figure 6).

Observations

Fa3l-s is the most commonly occurring and is made of several metre-thick intervals between undeformed turbidites (Figure 6). These intervals mostly comprise contorted turbidite beds (*e.g.,* recumbent folding) and sometimes include dislocated, pebble- to boulder-graded clasts of turbidites, within a silty mudstone background facies (Figure 6; Figure 8a, d, e, f, g, h). Towards the top of the turbidite system, most of the contorted strata indicate a SW apparent direction of movement. Overall, **Fa3l-s** is characterised by a good lateral continuity and thus its occurrences are easily followed across the outcrop. It often seems adjacent to **Fa1g-f** (Figure 6; Figure 8a, b).

Fa3l-d was only observed once (Figure 8h, lower MTD) and is characterised by a matrix-supported deposit containing at least 50% of intraformational clasts. They are mostly made of pebbles to outsized clasts (deci- to decametric) of turbidites. A couple of skeletons belonging to Molluscan species (*e.g.,* gastropods) were also locally observed, floating in the matrix.

Interpretations

Fa3l-s is interpreted to represent small-scale MTDs resulting from sliding and or slumping of initially coherent turbidite beds under the action of gravity (Nardin et al. 1979; Nemec 1990). The recurrence of these deposits suggests a generally unstable slope whereas their size, extent and nature imply a rather local source of input. The directions of mass-movements are fairly consistent and would indicate a slope that dipped to the SW (Woodcock 1979; Alsop et al. 2019), thus reinforcing the hypothesis of a ridge that was contemporaneously developing to the NE of Sefton Hills. The high sedimentation rates observed in the turbidite deposits (Table 1) can increase the prospect of depositing water-rich and mechanically weak sediments, more prone to fail along an unstable, rising slope (Lee 2009). We therefore interpret **Fa3l-s** as the result from local failures of the recently deposited turbidites (**Fa1g**) while the topography rose to the NE. **Fa3l-s** sometimes seems to laterally evolve from the lobe fringe deposits, thereby suggesting potential preferential destabilisation of these deposits. Finally, we interpret **Fa3l-d** to represent small-scale MTDs resulting from the transformation of **Fa3l-s** into a cohesive flow as it moved downslope (*e.g.,* Strachan 2008).

5.1.3. Shelf-derived mass-transport deposits

The upper part of the Sefton Hills outcrop is characterised by six distinct matrix-supported deposits, coalescing to over 100 metres of total vertical thickness and 50 to 80 metres of lateral continuity (Figure 6). They can be separated into two stacked sets of the same three main lithofacies (Figure 10) deposited in the same order (Figure 6). Despite erosional and sharp bases, one set essentially evolves between matrix-supported deposits containing a high-density (lithofacies **DF**) to a more diluted, dispersed amount of gravel-grade sediments (lithofacies **MF-1** and **MF-2**), thus displaying a general fining upward trend. The matrix of these deposits is made of light grey, silty mudstone and mostly contains extraformational clasts of pre- and syn-subduction material, in varying quantities, sizes and shapes.

Lithofacies Debris Flow (DF)

Observations

DF is a disorganised, poorly-sorted polymict conglomerate comprising ~50% of matrix. Its basal surface is sharp and slightly (<30 centimetres) to highly erosive into the underlying gravity-driven deposits (Figure 6).

In **DF**, pre-subduction material largely dominates. It is mostly made of sub-rounded to rounded dark granules to pebbles of Lower Cretaceous Torlesse greywackes. The remaining pre-subduction material (less than 1%) includes sub-rounded pebbles and cobbles of Upper Cretaceous (*e.g.,* calcareous mudstones), Paleocene (*e.g.,* Waipawa black siltstones) and Eocene to Oligocene strata, as well as sub-angular pebbles of Cretaceous to Paleocene strata (Figure 10a, f). Some rare sub-angular cobbles of Lower Cretaceous Torlesse greywackes can also be found.

Clasts of syn-subduction material can be divided into lithoclasts and bioclasts.

Lithoclasts are characterised by pebbles to boulders (sometimes outsized: deci- to decametric) of coherent to dislocated turbidites of similar nature to the ones from the underlying turbidite system, boulders to outsized mud clasts, sub-angular indurated shell bed clasts and black pieces of organic matter (*e.g.,* wood) (Figure 9b, c, e; Figure 10b, c, d, e). SE-verging recumbent folds were measured throughout the contorted expression of some of the turbidites (Figure 6; Figure 9c; Figure 10c).

Bioclasts are abundant and composed of macrofossils mostly belonging to Molluscan species (*e.g.,* bivalves and gastropods) and rarely to Corals (details in Appendix 2). This bioclastic material can either be found: (1) as shell fragments, finely milled and dispersed in the matrix (Figure 10a); or (2) as skeletons, partly to mostly well-preserved (being one to eight centimetres long) and floating in the matrix (Figure 10a, g). *Struthiolaria (Callusaria) callosa*, *Polinices* sp. as well as *Turritella* sp. were identified as the most recurrent macrofossil species of gastropods. Most of the bivalve shells appear to be only partially well-preserved, thereby making it complicated to classify some of the species; *Glycymeris* sp., *Cardium* sp. and *Ostrea* sp. were recognised.

Despite their common characteristics, differences exist between the two occurrences of the lithofacies **DF** at the Sefton Hills locality. The diversity encountered in the pre-subduction clasts decreases drastically in **DFb**. Lower Cretaceous Torlesse greywackes still dominate and are also locally particularly abundant (Figure 10a) whereas only a few Cretaceous to Paleocene clasts (*e.g.,* calcareous mudstones) are present. In terms of syn-subduction material, the mud clast content largely increases towards the top of **DFa** (Figure 10d) while this crude sorting does not exist in **DFb,** which records decametric, randomly scattered mud clasts (Figure 9b, e). The transported turbidites evolve from outsized, sometimes overturned rafts (Figure 9f; Figure 10b) to contorted and then dislocated cobbles and or boulders towards

391 the top of **DFa** (Figure 10c), whereas **DFb** is mostly made of dislocated, randomly scattered cobbles to
392 boulders. Both contain several types of shell bed clasts that are typically sub-angular, range from five to
393 20 centimetres in length and constitute a major part of the overall syn-subduction clasts at the base of
394 **DFa**.

395 Finally, the taphonomic analysis of the macrofossil content (Figure 12) shows that bioerosion contrasts
396 markedly between facies **DFa** and **DFb**, being overall low to moderate (combined frequencies of 78.2%
397 to 100%) for both the coarser and the finer skeletal fraction. Fragmentation, for grains larger than three
398 centimetres that include whole skeletons and partly broken ones, is similar within both facies, being
399 predominantly low to moderate (cumulated frequencies of 76.2% and 87%, respectively). Unsurprisingly,
400 fragmentation is high to very high for the finer skeletal fraction dominated by clastic material. The coarser
401 skeletal fractions in facies **DFa** and **DFb** exhibit similar degrees of abrasion (cumulated frequencies for
402 low to moderate abrasion is 71.4% in **DFa** and 60.9% in **DFb**, and for high to very high degrees of
403 abrasion, 28.6% in **DFa** and 39.1% in **DFb**). Interestingly, abrasion for the finer skeletal fraction is higher
404 in **DFa** than in **DFb** (high to very high degrees of abrasion of 33.8% and 16.6% respectively; Figure 12).
405 Macrofaunal assemblages and bioclastic remains are remarkably similar in facies **DFa** and **DFb**. At
406 outcrop scale, concentration of well-preserved skeletons in **DFa** may appear higher than in **DFb**. The
407 square metres of outcrop investigated for the taphonomic analysis show no difference in the
408 concentrations of well-preserved skeletons between both facies. However, the overall bioclastic content
409 is more abundant in **DFa** than in **DFb** (Figure 12).

410 *Interpretations*

411 **DF** is interpreted to represent a MTD produced by cohesive debris flows (*sensu* Mulder and Cochonat
412 1996; Mulder and Alexander 2001). The disorganised and chaotic arrangement is characteristic and the
413 predominance of matrix in the deposits indicates that matrix strength was the dominant grain-support
414 mechanism for the failed material (Nardin et al. 1979; Lowe 1982). Grain interactions may also be locally
415 important due to the abundance of coarse lithoclastic material.

416 The erosive nature of the deposits and presence of allochthonous, rafted blocks of contemporaneous
417 Miocene turbidites, sometimes completely overturned, at the base (cf. **DFa**) suggest basal interaction
418 between the overriding mass-flow and the substrate. Erosional ploughing and scouring is a common
419 feature of MTDs (Posamentier and Martinsen 2011; Festa et al. 2019) especially when hydroplanning
420 (*sensu* Mohrig et al., 1998) is not seen as the main mechanism responsible for the mobility of the flow.

421 The sedimentary rocks of the substrate are thus incorporated into the overflowing MTD by basal erosion
422 (Posamentier and Martinsen 2011; Sobiesiak et al. 2018). The crude grading observed in their shape and
423 size (outsized clasts to pebbles; raft to contorted or dislocated turbidites) throughout **DF** suggests layer-
424 parallel shearing within the flow. As the flow moved downslope and further substratum material was
425 added, it first remained coherent before partly disaggregating and starting to shear and deform in the
426 direction of the flow (Fonnesu et al. 2016). Alternatively, deformation could result from shearing and
427 compaction after the freezing of the flow (Mulder and Alexander 2001). The SE-verging measurements
428 collected in the contorted turbidites indicate a mass-flow travelling southward, likely parallel to the NW-
429 SE sublinear topography that developed to the NE of Sefton Hills (see 5.1.1 and 5.1.2).

430 Although **DFb** is also characterised by an erosional base, only a small amount of turbidites (of pebble- to
431 cobble-grades) are present. Large-scale mud clasts dominate throughout, thereby suggesting a change
432 in the nature of the underlying substratum being ploughed. **DFa** is the first episode of debris flow recorded
433 at Sefton Hills right above a well-developed turbidite system (Figure 6) whereas **DFb** is the second
434 episode. At least another two MTDs were recorded in between the two debris flows (Figure 6, cf. **MF-1a**
435 and **MF-2a**), thus providing an entirely different substrate (*i.e.,* mud-rich) to be eroded and incorporated
436 into the flow for **DFb**. Mud clasts are also present in the first debris flow although smaller and concentrated
437 towards its top (Figure 9b, e). These could be the result of hydraulic jumps at the time the debris flow
438 reached the base of slope (Henstra et al. 2016) or as it travelled above the uneven basin-floor topography.

439 The variety of lithoclasts and bioclasts encountered in **DF** illustrates the level of internal heterogeneity
440 usually associated with debris flows (*e.g.,* Mulder and Alexander 2001) and also provides insights about
441 the nature of the failed source area (Posamentier and Martinsen 2011). The quantity and diversity of pre-
442 subduction clasts suggest that the event of mass wasting did not only destabilise the sediments that were
443 being deposited in the source area (*i.e.,* Lillburnian sediments), but that the substratum onto which they
444 were depositing was remobilised as well. The nature of the clasts implies that this substratum mostly
445 comprised the pre-subduction series (*e.g.,* Cretaceous up to Oligocene) (Chanier 1991; Chanier and
446 Ferrière 1991). Yet, the few occurrences of Miocene shell bed clasts indicate that it also comprised some
447 syn-subduction sedimentary rocks previously deposited in shallow-marine, mixed siliciclastic-carbonate
448 environments (Chanier 1991; Bailleul et al. 2007; Bailleul et al. 2013; Caron et al. 2019; Bailleul et al.
449 Submitted; Caron et al. 2021).

450 The macropalaeontological analysis conducted onto the sampled fauna indicates a neritic shelfal
451 environment whereas the micropalaeontological data reveal that the deposition of the debris flow

occurred at lower bathyal depths (>1000 metres), with a planktic abundance varying from >80 to >95%, thus indicating deposition in a sub-oceanic to fully oceanic setting.

The taphonomic analysis suggests that the first event of mass wasting (**DFa**) remobilised macrofaunal assemblages that were either alive or only recently deceased on the shelf floor, whereas the second event (**DFb**) transported organisms that were, for most part, already dead and bio-eroded. Since the nature of the macrofossils transported in **DFa** and **DFb** remains the same, a repeated destabilisation of the same sourcing region can be inferred, with not enough time between the two events for the molluscan communities to replenish the neritic zone, *i.e.,* shelfal environment.

Mass-wasting is therefore interpreted to have initiated in shallow waters, from potential failure of a shelf that developed above a substratum composed of both pre- and syn-subduction material. The coevally developing shallow-marine, mixed siliciclastic-carbonate shelves to the north of Sefton Hills are great candidates for being the source, having formed on a pre- (*e.g.,* Upper Cretaceous to Paleogene series) and syn-subduction (*e.g.,* Miocene sediments) substratum (Figure 3, section f, i, m, p) (Bailleul et al. 2007; Bailleul et al. 2013), and presenting markedly similar faunal assemblages, which include *Struthiolaria* sp., *Polinices* sp., Turritellids, *Glycymeris* sp., Oysters or some Corals (Bailleul et al. Submitted). The destabilised material was then transported downslope and resulted in deposition of **DF** at deeper waters, into the Whareama Basin.

Finally, the high percentage (>30%) of sub-rounded to rounded, granules and pebbles of Lower Cretaceous Torlesse greywackes unlikely results from the underwater substratum. Instead, it might either come from (1) direct erosion of the hinterland that mostly comprises exhumed Torlesse rocks and or (2) reworking of Upper Cretaceous conglomerates, known to already contain sub-rounded granules and pebbles of Lower Cretaceous Torlesse greywackes, previously reworked through fluvial processes (Chanier 1991; Chanier and Ferrière 1991). Indeed, several shelfal deposits were described as containing sub-rounded pebbles to boulders of Torlesse greywackes (*e.g.,* in the Middle Miocene shelfal series of Oumukura (Chanier 1991) and in the Pliocene limestones of Hawke's Bay (Caron et al. 2004)), thereby indicating that Torlesse material, either already reworked or recently eroded, can likely be transported from the hinterland onto a shallow shelf, where it is then exposed to littoral processes. The presence of wood fragments in the deposits also indicates a connection (continuous or not) with an emerged land (Kuenen 1964), which could have also been used to bring and store the reworked sub-rounded Torlesse clasts into the source area.

Lithofacies Mudflow 1 (MF-1)

Observations

MF-1 is another type of disorganised, poorly-sorted polymict conglomerate. It is primarily distinguished by its high matrix content (~95%) and its resemblance to a diluted version of the lithofacies **DF**. It has a sharp, undulating basal surface, that laterally evolves into becoming highly erosive (decametric) towards the south (Figure 6, cf. **MF-1a** and **MF-1b**, Figure 9a, b, c, d, e, h; Figure 10h).

Pre-subduction material is largely dominant in **MF-1,** with a very high proportion of sub-rounded to rounded Lower Cretaceous Torlesse greywackes of very coarse sand to granule grades (Figure 10h). Cobbles and boulders of Cretaceous to Paleocene clasts are rarely found scattered in the matrix (Figure 10l).

The variety of syn-subduction lithoclasts is comparable to that of the **DF** lithofacies, and includes Miocene turbidites, shell bed clasts, organic matter (*e.g*. wood) and some mud clasts. It also punctually includes clasts of the underlying **DF** material. In general, the shell bed clasts and wood fragments (>1% of the total contribution) do not exceed pebble grades and are mostly sub-angular, and rarely sub-rounded (Figure 10k).

The bioclastic content remains important, however this material is now mostly found as shell fragments dispersed in the matrix (Figure 10h). A few (well- and partly-) preserved molluscan skeletons were identified (Figure 10m); gastropods tend to be the best preserved (details in Appendix 2).

We performed a taphonomic analysis on the finer skeletal fraction of **MF-1a** related deposits, the coarser fraction (*i.e.,* >3 centimetres) being virtually absent (Figure 12). Degrees of fragmentation range from high to very high. Overall, abrasion is low to moderate (45.6% and 50%, respectively; cumulated frequencies of 95.6%). Bioerosion is predominantly low (84.8% of no- or poorly-infested bioclasts) to moderate (10.9%).

The two occurrences of the lithofacies **MF-1** display quasi-similar characteristics at the Sefton Hills locality. The main difference affects the incorporated syn-subduction turbidites. In both cases, they are essentially characterised by pebbles to boulders of contorted to dislocated turbidites which can occasionally present bioclastic grits or laminations (Figure 9d, h; Figure 10i). A decametric mass of coherent thin-bedded turbidites (*i.e.,* raft) is however present at the top of **MF-1b** (Figure 9a; Figure 10i). It displays a high number of angles and truncations, and is wrapped by the matrix.

Interpretations

MF is interpreted as a MTD resulting from cohesive mudflow (*sensu* Mulder and Cochonat 1996; Mulder and Alexander 2001). The dominance of matrix suggests that cohesive strength (*i.e.,* matrix strength) was the dominant grain-support mechanism for the incorporated material in this lithofacies (Nardin et al. 1979; Lowe 1982). The presence of unusually large clasts (*e.g.,* turbidite decametric raft) floating on top of the flow is not uncommon in MTDs (Posamentier and Martinsen 2011). This occurrence indicates the presence of additional support mechanisms in **MF-1b** such as high local pore pressures, buoyancy and or clast-to-clast interaction (Pierson 1981; Johnson 1984; Nemec and Steel 1984; Postma et al. 1988; Mulder and Alexander 2001).

The nature of the reworked material (lithoclasts and bioclasts) is equivalent to that of **DF**, thereby suggesting destabilisation and remobilisation of a similar, if not identical, sourcing region. The macrofaunal species remain the same as the ones recorded in **DF** and thus indicate that the failure responsible for the deposition of **MF-1** destabilised a neritic shelfal environment as well.

The geometry and distribution of the basal incisions recorded in **MF-1** can be used to infer the gross general transport direction. Their characteristics suggest that the flow was moving almost perpendicular to the outcrop orientation along a NW-SE direction, with a migration of incision towards the south (Figure 6, cf. **MF-1a** and **MF-1b**). These incisions could either result from basal erosion (Posamentier and Martinsen 2011; Sobiesiak et al. 2018) or could be associated with the build-up of lateral margins (Bull et al. 2009; Posamentier and Martinsen 2011). In both cases, such features provide a primary constraint on the flow direction of the MTD and also indicate the potential position of the lithofacies within the MTD body and across the seafloor. Lateral margins and flow-ploughing commonly develop in the translational domain of the MTD body, which is located between the up and downslope extremes (*i.e.,* the headwall and toe domains) (Bull et al. 2009), outboard of the base of slope. In this domain, the MTD is characterised by intense deformation, dislocation, basal erosion as well as incorporating translated, rafted blocks (Frey-Martínez et al. 2005; Bull et al. 2009; Posamentier and Martinsen 2011), all being features of the **MF-1** lithofacies.

Lithofacies Mudflow (MF-2)

Observations

MF-2 is mostly made of light grey, silty mudstone (Figure 10n). The matrix represents 99% of the overall flow deposits and the remainder is divided between that with a high bioclast content and that with rare

scattered lithoclasts. The basal surface is sharp yet sometimes can appear as slightly gradational from **MF-1**.

MF-2 shows good lateral continuity (Figure 9a, g, h). For example, its second occurrence (**MF-2b**) can be traced over one kilometre from the southern part of the Sefton Hills section 1 locality to the Sefton Hills section 2 (Figure 9g).

In **MF-2**, the lithoclasts are rare and do not display much variety. In order of frequency, they are (1) a few syn-subduction decametric mud clasts, (2) rare syn-subduction pebbles to boulders of contorted and dislocated turbidites (Figure 10o) and (3) rare pre-subduction elements of sand sizes, likely of Lower Cretaceous Torlesse greywackes. Where dominated by mud clasts, **MF-2** can easily be mistaken for hemipelagic mudstones; but is differentiated based upon the matrix that surrounds the mud clasts laterally. The bioclasts are essentially shell fragments; only a couple of molluscan skeletons were found floating in the matrix, partly preserved yet highly disarticulated (details in Appendix 2).

Interpretations

MF-2 is also interpreted as a MTD resulting from cohesive mudflow (*sensu* Mulder and Cochonat 1996; Mulder and Alexander 2001). Its texture closely resembles that of lithofacies **DF** and **MF-1**, albeit in a very low-density version. Mass-transport processes can either be intergradational or not (*i.e.,* one process can evolve into another with time or remain the same) (Stow 1986; Nemec 1990). Sediment dilution through water entrainment, particularly at the head (Middleton and Hampton 1973) or at the upper boundary of a flow (Mulder and Alexander 2001) is known as a major mechanism contributing to the transformation of one cohesive flow into another (Lowe 1982; Mulder and Alexander 2001). Therefore, **MF-2** could represent the diluted expression of an initial debris flow (**DF**) or mudflow (**MF-1**). The low density of clasts may also indicate that either the source area was fairly depleted at the time of destabilisation or that the flow did not directly initiated from this location, but further downslope, from a muddier, deeper environment (*e.g.,* the upper- or mid-slope environment (Posamentier and Martinsen 2011)).

Once again, the clast content suggests the failure of a shelfal environment with a stock of reworked Torlesse clasts whereas the micropalaeontological study (Appendix 1, sample T27/f0643 taken in **MF-2b**) reveals that deposition remained at lower bathyal depths (>1000 metres). The mud clast content would have again resulted from the seafloor ploughing effects (Posamentier and Martinsen 2011; Sobiesiak et al. 2018) and thus points towards an erosive character of the flow.

5.1.4. Stratigraphic architecture of the Sefton Hills gravity-driven systems

Overall, the Sefton Hills outcrop is characterised by deposition of two main syn-subduction gravity-driven systems during the Middle Miocene, mid Lillburnian. The underlying turbidite system evolved from an unconfined, distal sheet-lobe setting (**Fa1s**) to a more confined and proximal depositional lobe setting (**Fa1g**) as a NW-SE sublinear topographic high developed to the north-east and isolated this part of the Whareama Basin from the unconfined basin floor to the east. Most likely controlled by the underlying seaward-verging Flat Point-Whakataki Fault complex, the rise of this topographic high not only resulted in the development of a SW-dipping slope (*i.e.,* backlimb setting) that deflected the incoming turbidity currents but also favoured repeated destabilisation of the syn-kinematic turbidites, thereby generating local gravitational instabilities leading to deposition of small-scale (one to five metres thick) MTDs (**Fa3l**).

This turbidite system was then abruptly interrupted by the emplacement of six amalgamated MTDs (**DFa, MF-1a, MF-2a, DFb, MF-1b, MF-2b**) that reworked a vast quantity of shelf-derived material. Together, they form a large-scale mass-transport complex (MTC) (**Fa3p-d**) of over a hundred metres in thickness, with up to a kilometre of lateral continuity. The nature of these deposits suggests the repeated failures of a shallow marine, shelfal environment developed above a substratum composed of both pre- and syn-subduction material, which also caught and stored land-derived elements (*e.g.,* reworked pebbles of Torlesse greywackes, wood and plant debris). Mass-failures likely initiated at shallow water depths north of the study area. The failed material then travelled southward, parallel to the Whareama Basin seaward margin, and downslope through erosive cohesive flows (*e.g.,* debris flow and mudflow). Deposition eventually occurred onto the Whareama trench-slope basin floor, above the Sefton Hills turbidite system, at greater water depths, *i.e.,* lower bathyal, and within southward migrating depocentres.

The two main gravity-driven systems of Sefton Hills are not genetically linked. Yet, they were fed by similar sources of material (shell fragments, wood and plant debris). Shoreline river systems could have directly supplied land- and beach-derived material to the shelfal domain (Posamentier and Walker 2006) making it readily available to be transferred beyond the shelf edge and farther downslope, either caught (1) in canyon heads, generally ending their course downslope into turbidite systems (Posamentier and Allen 1999) or (2) in unconfined shelf edge failures, resulting in large-scale MTDs (Moscardelli and Wood 2008; Moscardelli and Wood 2015).

The palaeocurrent variations recorded in both systems (north-eastward migrating turbidite system and southward MTDs) indicate that the shallow marine shelfal environment(s) located to the west of the Whareama system at the time was(were) persistent, well-developed and geographically extensive.

5.2. Te Wharau Basin

In this study, we also examined outcrops located in the main portion of the Te Wharau Basin (Figure 5, sections c and r) and in its easternmost secondary fold portion (Figure 5, sections tw-1, tw-2 and n). These outcrops expose additional occurrences of contemporaneous shelf-derived MTDs from the Middle Miocene, Lillburnian (Late Langhian to Serravallian, 15.1 – 13.05 Ma) (Appendix 1). Intermittent, these inland outcrops did not allow the same detail of descriptions and measurements as the coastal outcrops. Nevertheless, we were able to characterise each outcrop following the same approach and nomenclature defined at the Sefton Hills locality (Table 1; Figure 11).

We identified several occurrences of matrix-supported deposits identified in the Te Wharau Basin (Figure 5). Their apparent dimensions are of three to 20 metres of vertical thickness and 15 to 30 metres of lateral continuity. However, both the base and top surfaces could not be distinguished, thereby suggesting possibly greater thickness of deposits (Figure 11). They essentially hold similar general characteristics to those of Sefton Hills. Their matrix is made of light grey, silty mudstone and mostly contains gravel-grade extraformational clasts of pre- and syn-subduction origins (Figure 11a). Despite poor outcrop conditions, the deposits seem to hold between 30 to 40% of lithoclasts and bioclasts; which could imply that they are best defined by the lithofacies **DF** (Table 1).

Lithofacies Debris Flow (DF)

Observations

In the Te Wharau Basin, pre-subduction material also largely dominates the disorganised, poorly-sorted, polymict conglomerates of lithofacies **DF**. They mostly include Lower Cretaceous Torlesse greywackes, either as sub-rounded to rounded pebbles or sub-angular cobbles, boulders or outsized clasts (Figure 11a, c, d, f). The remaining pre-subduction material comprise sub-angular pebbles to outsized clasts (metric) of other Lower Cretaceous (*e.g.,* red cherts), undifferentiated Cretaceous (*e.g.,* calcareous mudstones) and Paleocene strata. The syn-subduction lithoclasts are essentially characterised by sub-angular pebbles to cobbles of shell beds (Figure 11b, c). Contorted turbidites are rarely found.

Bioclasts are abundant and composed of a large variety of Molluscan species (details in Appendix 2; Figure 11b, d, e) either found: (1) as shell fragments, finely milled and dispersed within the matrix or (2) as skeletons, partly to mostly well-preserved (generally two to three centimetres) and floating in the matrix. The gastropods are the best preserved, whereas the bivalves are commonly partly broken and chalky.

Despite some characteristics that are similar to those of Sefton Hills, the Te Wharau occurrences present some differences. Overall, the clasts are dominantly sub-angular. The largest clasts (*e.g.,* boulders) are found in the Te Wharau road-2, Ngaumu and Rangiora sections (Figure 5). In particular, pre-subduction material dominates at Ngaumu and Rangiora. It includes Lower Cretaceous Torlesse greywackes, Cretaceous calcareous mudstones and Paleocene glauconitic sandstones. At Ngaumu, Lower Cretaceous red cherts and lavas are also present. At Te Wharau road-1, the syn-subduction lithoclasts are represented by different types of shell beds. At Te Wharau road-2, both shell bed clasts, skeletal and bioclastic fine-grained sandstones (respectively the facies S1 described by Caron et al. (2004) and the facies Fa6b described by Bailleul et al. (2007)) are found (Figure 11e). At Ngaumu, the syn-subduction material comprises shell bed clasts along with rare scattered and contorted turbidites.

Interpretations

We interpret the different occurrences of **DF** observed in the Te Wharau Basin to be MTDs produced by cohesive, likely debris flows (*sensu* Mulder and Cochonat 1996; Mulder and Alexander 2001). Despite great internal heterogeneity, the extraformational clast content remains similar across the different occurrences, displaying the same types of pre- and syn-subduction material and thus demonstrating failures of comparable sources.

The nature of the lithoclasts, largely dominated by Lower Cretaceous material and Miocene shell bed clasts, suggests slightly different substratum(s) to the one(s) sourcing the contemporaneous MTDs of Sefton Hills. These substrata were made of Lower Cretaceous Torlesse greywackes and cherts, above which Middle Miocene shelfal environments developed, highlighting a substantial sedimentary hiatus.

During the Middle Miocene, Clifdenian (Early Langhian, ca. 15.9 – 15.1 Ma) and Lillburnian (Late Langhian to Serravallian, 15.1 – 13.05 Ma), a few episodes of mixed siliciclastic-carbonate shelves unconformably overlying Lower Cretaceous Torlesse basement were documented in the sector of Te Wharau, and more particularly at the Wainuioru and Mapapa stream localities (Figure 5, sections w, o, ms) (Crundwell 1987; Chanier 1991). Their failure could have directly provided the material for the macrofossil content, shell bed and Torlesse clasts recorded in the MTDs of the Te Wharau Basin (Figure 5). The rounded clasts of Torlesse greywackes probably resulted from fluvial and or littoral reworking of the material, initially exposed in the hinterland (Chanier 1991; Chanier and Ferrière 1991) and later transferred onto the shelfal environment.

Input from the pre-subduction Upper Cretaceous to Paleogene series are scarce and only clearly observed in the MTDs from the Ngaumu and Rangiora sections. Around these areas, owing to the Adams-

Tinui Fault complex (Figure 5), the Lower Cretaceous Torlesse basement overrides the Glenburn Nappe and thus locally provides a substratum that also includes the Upper Cretaceous to Paleogene series.

Finally, the micropalaeontological studies reveals that the deposition of the debris flows generally occurred at bathyal depths. More particularly, the Te Wharau road occurrence (section tw-1) indicates mid-bathyal water depths (700 metres), which are shallower than in the Whareama Basin, and the planktic abundance of 25% also indicates that an outer neritic water-mass was overlying the site of deposition at the time, thereby suggesting nearby shelfal source(s). Overall, the local source regions (maximum of seven kilometres distance from the known Wainuioru and Mapapa shelves) (Figure 5) support the prospect of the Te Wharau cohesive flow deposits being more proximal to their sources than those at Whareama.

6. DISCUSSION

6.1. Stratigraphic record of shelf-derived mass-wasting events at outcrop

The shelf-derived mass-wasting products presented in this study are captured across several exhumed trench-slope basins and exhibit a variety of lithofacies and geometries. They always incorporate reworked well-preserved to fragmented shallow marine macrofauna as well as (pre- and syn-subduction) extraformational clasts, suggesting the destabilisation and collapse of similar depositional environments. However, the diversity observed in the shapes, sizes, percentages of reworked material and the interactions with the underlying surface imply that different physical and sedimentary processes interplayed as the failed material moved downslope. Such variety also suggests that the deposits may have been recorded at different locations (*e.g.,* distance) relative to the source regions.

6.1.1. Source regions

The analysis of the macrofossil content (palaeontology and taphonomy) indicates that the staging areas were located at shallow depths in neritic shelfal waters. The analysis of the extraformational content also adds that the events remobilised the fauna and sediments that were depositing in the failed source area (*i.e.,* Middle Miocene, syn-subduction) as well as partially destabilised the substratum upon which they were settling (*i.e.,* syn- and or pre-subduction material). The contemporaneously developing shallow-marine, mixed siliciclastic-carbonate shelves, markedly installed above pre- and or syn-subduction substratum and presenting similar faunal assemblages are thus great candidates for the source regions

(Figure 3, sections f, i, m, ms, p, t, w) (Crundwell 1987; Chanier 1991; Bailleul et al. 2007; Bailleul et al. 2013; Bailleul et al. Submitted). The failed material was then transported downslope into deeper water settings, being deposited either along the main slope, proximally to the source area (*e.g.,* Te Wharau road MTDs) or onto the trench-slope basin floor, further from the source and at lower bathyal water depths (*e.g.,* Sefton Hills MTDs). The land-derived material (*e.g.,* wood fragments, reworked sub-rounded pebbles) captured in these deposits probably results from the uplift and erosion of hinterland areas, which typically transfer such material to the coastal and shelfal environments, making it readily available to be incorporated into the failed deposits. Isolated islands developed above tectonically controlled topography can also be considered for providing plant material (McArthur et al. 2016).

6.1.2. Taphonomic insights

A key question related to the taphonomic character of the shelfal skeletal sediments contained in the studied MTDs and presented in Figure 12, is as to whether they were inherited or, at least partly, acquired during transport and emplacement of the MTDs. Explanations for limited bioerosion of skeletal material are multifarious, including unfavourable ecological conditions for bioeroders, substrates unsuitable to drilling organisms, high fine-grained siliciclastic inputs, increasing water depths, predominance of organisms buried alive and rapid burial preventing infestation (*e.g.,* Kidwell 1989; Perry 1998; Martin 1999; Richet et al. 2011). Notwithstanding the possibility for fragmentation to be related to biotic factors (*e.g.,* Zuschin et al. 2003), the degrees of fragmentation and abrasion may help assess whether flows were either laminar or turbulent, and whether sediments were deposited by traction or suspension (*e.g.,* Lowe 1982). Due to the abundance of coarse lithoclastic material in the lithofacies **DF**, there is a potential for fragmentation to have originated from *en masse* crushing during transport, and abrasion to reflect *en masse* friction as possible mechanisms by which skeletons were altered. Fragmentation during transport of previously broken and abraded material will lower its taphonomic evaluation because this secondary mechanical event generates new angular edges. This process may explain why abrasion values compare well in the various size fractions of lithofacies **DF**. In contrast, the abundance of silty mudstone matrix and the low siliciclastic content in lithofacies **MF**, hence reducing *en masse* friction between grains and making crushing unlikely (*e.g.,* Li et al. 2019), may explain their limited abrasion and could indicate that abrasion and fragmentation were inherited.

6.1.3. Distance to source and facies

In the Te Wharau Basin, we interpret the Te Wharau road cohesive flows to represent the fairly proximal and immature expressions of the failure, captured close to the sourcing area(s), most probably on the

slope. The disorganised clast fabric may reflect short travel distance (Nemec and Steel 1984) whereas the high density of angular, boulder-grade clasts could also suggest a rather recent mobilisation (*sensu* Iverson 1997).

Further north, in the Akitio Basin, a 175-metre thick series of large-scale slides and slumps (cf. **Fa3p-s** in Table 1) interbedded with a few cohesive flows, similar in nature to the ones of the Te Wharau Basin, were also observed (Branscombe MTDs of Bailleul et al. (2007)). These MTDs deposited in proximal position to the contemporaneously developing mixed siliciclastic-carbonate outer shelf of Pongaroa (Figure 3, sections b and p) (Bailleul et al. 2007; Bailleul et al. 2013) and thus indicate that both sediment mass-failure (*e.g.,* Akitio) and mobilisation (*sensu* Iverson 1997) (*e.g.,* Te Wharau) can occur close to the source areas.

In the Whareama Basin however, the cohesive flows captured at Sefton Hills deposited farther from the sourcing shelf area(s), at lower bathyal water depths onto the trench-slope basin floor. More importantly, the Sefton Hills deposits are characterised by amalgamated cohesive flows that can result from several failures that coalesced downslope. In particular, we observed repeated sequences of coalescing, erosive flows that display a rough fining upward trend (**DF**: debris flow, to **MF-1** and **MF-2**: mudflows in Figure 8 and Figure 10). Debris flows do not always move downslope as one single flow and commonly break into a series of surges (e.g., Iverson 1997; Mulder and Alexander 2001; Felix et al. 2009; Allen et al. 2020). One flow event can therefore be characterised by a multitude of surges, either arising naturally (*e.g.,* induced by surface wave coalescence (Iverson 1997)) or initiated by external triggers such as sporadic slope failures. Here, each failure would have triggered the development of a cohesive flow, breaking up downslope into at least three separated surges. During multiple-surge events, the first surge is usually the coarsest one, then tailed by surge(s) of medium and finer particles behaving as muddy flow(s) (Zanuttigh and Lamberti 2007). Consistent replications of grading and structure divisions can be expected in such deposits, and we therefore infer that the Sefton Hills deposits recorded two main events of shelf destabilisation (event a and b), each divided into three genetically-linked surging flow deposits (lithofacies **DF**, **MF-1** and **MF-2**).

As such, the shelf-derived deposits presented in this study indicate that shelf failures triggered both sediment mass-movement (**Fa3p-s**) and development of debris flows (**Fa3p-d**) close to the source region(s) (*e.g.,* Akitio and Te Wharau MTDs), which may eventually break down into a series of erosive, upward fining surges downslope (*e.g.,* Whareama MTDs) (*e.g.,* Figure 13).

6.1.1. Deposit dimension and scale

The source regions, regional footprint and internal characteristics of these MTDs all suggest that they belong to *attached* systems sourced from the shelf (Moscardelli and Wood 2008; Moscardelli and Wood 2015). In order to better comprehend the full three-dimensionality and extent of these shelf-derived mass-wasting deposits at outcrop scale, we used the set of morphometric relationship equations calculated by Moscardelli and Wood (2015) as a basis for reconstructing their potential dimensions.

We used the best outcropping occurrences of Sefton Hills (Whareama Basin) and Branscombe (Akitio Basin) as references, having access to representative thickness estimations from fieldwork measurements. We considered whether or not these MTDs were part of the same event or had a coeval trigger (*e.g.* a megathrust earthquake); yet, we rapidly discarded this hypothesis since the micropalaeontological analysis showed that they were not contemporaneous; the Branscombe MTDs being slightly older (lower Lillburnian) (Bailleul et al. 2007; Bailleul et al. 2013).

The resulting morphometric calculations, whether using the general or specific set of equations, provided volume, area and length values that are generally above the generic thresholds for *attached* systems (Moscardelli and Wood 2015) (*i.e.,* V >1 cubic kilometres; A >100 square kilometres and L >11 kilometres (Figure 14; Appendix 4), thereby reinforcing such an interpretation of these MTDs.

In addition, we considered the average deposit length parameter (*sensu* Moscardelli and Wood 2015) to account for the lateral thickness variations that are typical of MTDs and gain additional insights onto the possible source areas, especially those of the Sefton Hills MTDs. Notwithstanding the presence of potentially closer source regions, yet to be discovered in the studied area, we used the shortest distance between the deposits and the already well-known shelfal areas as a proxy (Appendix 4). The results favour a potential source region located 40 to 70 kilometres to the north, nearby the Tinui, Takiritini or Waihoki-Mangatiti shelves (Figure 14; Appendix 4). However, these results should only be considered as general insights since the Sefton Hills deposits have not been proven to be the termination of the MTDs, the input deposit lengths do not account for possible tortuous pathways or closer source regions, the deposit thickness does not take into account potential compaction effects, which can be substantial in muddy sediments (Jones 1944), and the outcrop conditions hindered their full exposure (*e.g.,* upper bounding surface is not visible).

Interestingly, the MTDs from the Te Wharau Basin show contrasting results that suggest the coeval presence of smaller (*i.e., detached*) systems (Figure 14; Appendix 4). The limited outcrop exposures may explain such results, preventing the recognition of representative thickness values. Yet, the potential

783 presence of isolated shelves (*e.g.,* Caron et al. 2021) and or the particular geotectonic settings and
784 triggering mechanisms evidenced for the shelf-derived MTDs we present in this study (*i.e.,*
785 oversteepened slope due to thrust activity), which contrast with the causal mechanisms traditionally
786 invoked for shelf failure (*e.g.,* sea-level changes, high-sedimentation fluxes) (see 6.2), should also be
787 taken into account. Whilst oversteepened slopes at the thrust fronts (*e.g.,* forelimb settings) appear to
788 generally source reduced MTDs volumes (~V <5 cubic kilometres) (*e.g.,* Watson et al. 2020), the complex
789 interactions that exist between sediment supply, slope profile and shelf width along convergent margins
790 can also alternatively promote the development of *attached* or *detached* systems from regional slope
791 settings (*e.g.,* shelf) (*e.g.,* Naranjo-Vesga et al. 2020). Therefore, although further work is required to
792 generalise such observations and interpretations to our study area, the different styles and sizes of shelf-
793 derived MTDs described in this study rather support the prospect of slightly more complicated
794 morphometric relationship and classification along tectonically active margin settings, whereby the shelfal
795 region may contemporaneously source both *attached* and *detached* systems.

796 Overall, the morphometric values suggest seismic-scale shelf-derived MTDs throughout the study area.
797 Traditionally, the seismofacies of mud-dominated cohesive flows is defined by low amplitude, semi-
798 transparent and chaotic reflections (Bull et al. 2009). Here however, we cannot expect for the internal
799 architecture of the Sefton Hills MTC, as described in this high-resolution study (*i.e.,* several coalescing
800 shelf-derived MTDs), to be imaged by the seismic data because of resolution limitations. A mud-
801 dominated deposit containing clasts, whether milli-, deci- or decametric or having contrasting
802 concentrations, would hold similar acoustic impedance characteristics and thus look the same at seismic
803 scale. Therefore, the coalescing shelf-derived MTDs of Sefton Hills will be imaged as one unique MTD
804 (seismofacies) at seismic-scale, thereby missing the potential discrete, multiple-surge events responsible
805 for deposits holding distinct lithological and petrophysical properties at outcrop-scale.

806 6.2. Causes and controls for continued destabilisation of source regions

807 We previously demonstrated that the MTDs described in this study were sourced from the destabilisation
808 of the contemporaneously developing shelfal environments. Gravity-driven instabilities can however
809 result from a variety of processes, and fortunately, the MTDs characteristics (*e.g.,* geomorphologic
810 features) provide direct evidence on the former failure processes and basin settings (Mulder and
811 Alexander 2001; Bull et al. 2009; Posamentier and Martinsen 2011; Talling et al. 2012). Accordingly,
812 shelf-derived MTDs are generally inferred to be controlled by extrabasinal, regional-scale processes;
813 notwithstanding gas-hydrate dissociation, storms, longshore currents or tectonic activity (*e.g.,*

earthquakes) as other important causal mechanisms, relative sea-level changes and high sedimentation fluxes remain the most commonly invoked triggers (*e.g.,* Posamentier and Kolla 2003; Moscardelli and Wood 2008; Moscardelli and Wood 2015; Bull et al. 2020).

The nature and size of the remobilised material presented here indicates powerful events that destabilised both the shelf substratum and fresh sediments. The resulting products, recorded across several trench-slope basins (along a 70 kilometre-long transect), point towards a margin-wide episode of destabilisation leading to a regional footprint of the associated deposits. The different ages captured in the MTDs (*e.g.,* T27/f632: mid Lillburnian; T27/f638: early Lillburnian) however argue for a period (rather than a single, brief episode) of widespread failure that lasted ca. 1 to 2 Ma. The Sefton Hills MTDs also add that within this period, a series of close, high-frequency collapse events (*i.e.,* multi-surge events) repeatedly occurred.

At global scale, the sea-level changes highlighted a couple of drops during the Middle Miocene, Lillburnian (Haq et al. 1987; Miller et al. 2005) that may have punctually influenced the stability of the shelf(ves). However, although shelf edges are commonly steep already (Schlager and Camber 1986) and thus prone to both oversteepening and failure, no statistically significant link or pattern seem to exist between the sea-level changes and occurrences of slope failure (Urlaub et al. 2013). Conversely, sea-level variations will generally have a major impact on seafloor pressures (*e.g.,* hydrostatic pressure) and temperatures (*e.g.,* warm currents) (Urlaub et al. 2013). An increase in temperature of as little as 1°C at water depths <600 metres (*e.g.,* shelf) can shift the gas hydrate stability zone downslope, engender dissociation of the hydrate accumulation, release substantial quantities of free gas and thus promote slope failure (Reagan and Moridis 2008). Widespread evidence of gas-hydrate deposits exists in the Hikurangi Margin; however, it is unclear whether these deposits already existed during the Middle Miocene. Moreover, Moscardelli and Wood (2008) and Moscardelli and Wood (2015) trust that gas-hydrate dissociation preferentially leads to the catastrophic failure of a large sediment volume (rather than a succession of failures), thereby discarding it as a potential cause for the MTDs described in this study. Storm-induced waves and longshore currents are also known to potentially trigger slope failure in shallow waters. In the Akitio Basin, the Middle Miocene Pongaroa shelf displays a shallowing-up trend capped by storm-influenced deposits (Bailleul et al. 2007). However, the related sedimentary features are of too small a magnitude (*i.e.,* two to 10-centimetre-thick shell lineation in 30 to 50-centimetre-thick shell beds) to suggest a powerful event responsible for large-scale destabilisation. The duration of such event, although greater than that of an earthquake, also does not explain the recurrence and surges that were observed in some of the deposits. Also, no indication of contour current deposits has ever been reported on this margin during the Middle Miocene, thereby ruling out this other mechanism.

On the Hikurangi Margin, shelves commonly formed in association with margin uplift and are located above tectonically induced stratigraphic surfaces (*e.g.,* angular unconformities) resulting from rapid motion of the basins' margins (Bailleul et al. 2013). For example, the Pongaroa and Waihoki-Mangatiti shelves developed above silty deep-marine deposits (Bailleul et al. Submitted). Interestingly, the angular unconformities not only appear to be coeval with the accumulation of the first shelfal sediments but can also be correlated with the remobilisation and deposition of the associated MTDs along the slope and into deep-water settings. The tectonic activity related to the development of basin-bounding structures (*e.g.,* thrusts) follows timescales of ca. 1 to 2 Ma (Nicol et al. 2002; Bailleul et al. 2013). Therefore, these short tectonic periods have not only recorded discrete, high amplitude structural movements (*e.g.* uplift) responsible for dramatic changes in depositional environments (*e.g.,* neritic conditions) (Figure 15). They also most likely controlled the continuous (with or without break) propagation of the associated thrust fault(s) and thus favoured the development of abrupt, unstable areas near the shelf edges (*e.g.,* forelimb setting).

High sediment fluxes, known to fundamentally modify the dynamic equilibrium of an area and influence the growth of (pre-existing) structures (Storti and McClay 1995; Malavieille 2010; Graveleau et al. 2012; Barrier et al. 2013; Noda 2018) could have also contributed to some of the oversteepening. Hence, we attribute the above-described shelf-derived MTDs to be primarily controlled by tectonic uplift and oversteepening. These findings are in agreement with those of Watson et al. (2020) (although built from the analysis of MTDs sitting on the seafloor), who proposed for these two mechanisms to be mainly responsible for the mass-wasting processes occurring along the Hikurangi Margin thrust ridges. We here bring new insights as to some of the depositional environments being destabilised by these mechanisms in the older stratigraphic record.

Finally, vertical movements of the coastline can also result from earthquakes (Pilarczyk et al. 2014) and the Hikurangi Margin has a history of both subduction and upper plate fault earthquakes (Clark et al. 2019). The accompanying co-seismic shaking can trigger large-scale subaqueous slope instabilities and the subsequent generation of gravity-driven flows (*e.g.,* MTDs) (Hampton et al. 1996). A series of tsunamigenic waves (*i.e.,* series of surges) can also be induced, resulting in the seaward downslope transport (tsunami backwash) of a wide range of material from terrestrial (*e.g.,* organic matter) to shelfal (*e.g.,* mollusc macrofossils) origins; and despite high-energy transport, the fossils can remain taphonomically unaltered (*i.e.,* pristine) (Einsele et al. 1996; Pilarczyk et al. 2014). However, no seaward to landward current reversals nor violent fluid escape features, characteristics of tsunamites (Dawson and Stewart 2007), were observed in our deposits.

Watson et al. (2020) argued against ground shaking as a primary control in thrust-related mass-wasting processes. Although ground shaking is undoubtedly important, we also believe that for the MTDs described in this study, this process may not be the primary (but a secondary) control. We interpret periods of repeated tectonic activity (thrust propagation and uplift) to be the main causal mechanism for shelf destabilisation and collapses (Figure 15). Continued (ca. 1 to 2 Ma) tectonic activity (possibly combined with earthquake(s)) would lead to recurring generation and destruction of oversteepened slopes. The shelf-edge escarpments would thus be repeatedly destabilised, allowing for the development of multiple episodes of mass-wasting along the margin. Like other mechanisms, such as gas-hydrate dissociation or storm-induced waves, sea-level changes and high sedimentation rates, commonly inferred to be the dominant causal mechanisms, most likely contributed to some mass-wasting, punctually influencing the stability of the shelf(ves), however they did not act as the main triggers for the shelf-derived MTDs described here.

6.3. Implications for the Coastal Ranges and active Hikurangi Margin

A number of mixed siliciclastic-carbonate shelfal environments coexisted in the Coastal Ranges during the Middle Miocene, Lillburnian (Crundwell 1987; Chanier 1991; Bailleul et al. 2007; Bailleul et al. 2013; Bailleul et al. Submitted) and their linear distribution along a 120 kilometre-long, NE-SW transect (Figure 3; Figure 5) indicates that they most likely formed a regional continental shelfal domain in the south-western portion of the Hikurangi Margin at the time. The high amount of land-derived material (*e.g.,* organic matter, reworked sub-rounded pebbles), incorporated in both the shelfal and resulting MTDs, is in favour of a narrow, continent-attached system receiving regular terrigenous input from the hinterland areas. No lateral continuity has yet been established between the different locations, therefore development of partially connected or isolated, continent-detached platform systems upon and about actively fault-growing folds (Caron et al. 2004; Caron et al. 2021) may have also locally occurred (*e.g.,* (Bailleul et al. 2013), Fingerpost shelf).

The diversity observed in the nature of the reworked material (*e.g.,* clast content, size) and the regional footprint of the MTDs suggests destabilisation of most, if not all, of these platforms (Figure 16). These shelves developed above substantially different substratum inherited from local tectonics, thereby allowing us through the thorough analyses of the reworked material to retrace the potential sourcing region(s) of the different MTDs recorded in the trench-slope basins (see 5.1.3, 5.2, 6.1). The northern shelves from the Akitio Basin (Figure 3, sections i, p, m, t) most likely sourced the Branscombe and southward-moving Sefton Hills MTDs respectively captured in the Akitio and Whareama Basins (Figure

3; Figure 16; sections b, s), whereas the southern shelves of Wainuioru and Mapapa (Figure 3; Figure 16; sections ms, w) are great candidates for the MTDs recorded in the Te Wharau Basin (Figure 3; Figure 16; sections c, n, r, tw). Therefore, the Middle Miocene, Lillburnian, not only staged the development of regional shelfal domain(s) across the south-western portion of the Hikurangi Margin (Crundwell 1987; Chanier 1991; Bailleul et al. 2007; Bailleul et al. 2013; Bailleul et al. Submitted) but they also recorded their coeval destabilisation and failure(s) (Figure 16).

The Akitio and Whareama Basins were connected during the Early Miocene (Bailleul et al. 2013), and this connection most probably persisted, at least partially, during the Middle Miocene to allow for some of the mass-wasting products sourced from the Akitio shelves to travel southwards into the Whareama Basin (*e.g.,* Sefton Hills MTDs) (Figure 16). We therefore propose that the seaward margin of the Akitio Basin, partially emerged at the time (*i.e.,* Cape Turnagain Structural High), formed together with the seaward margin of the Whareama Basin a rather continuous topographic barrier (emerged or submerged) to the east, most probably in the southward continuation of Cape Turnagain (Figure 16). Such ridge was likely controlled by the underlying Whakataki-Turnagain Fault complex to the north, laterally evolving into the Flat Point-Whakataki Fault complex to the south (Figure 3).

Finally, from ca. 15 Ma, the Hikurangi Margin is inferred to have undergone a major change in tectonic regime, entering into a period of generalised subsidence, after 10 Ma of active folding and reverse faulting (Chanier and Ferrière 1989; Chanier and Ferrière 1991; Rait et al. 1991; Chanier et al. 1999; Nicol et al. 2002; Bailleul et al. 2007; Nicol et al. 2007; Bailleul et al. 2013; Malie et al. 2017; McArthur et al. 2019). However, we just demonstrated (see 6.2) that the southern portion of the Hikurangi Margin was still dominated by shortening and uplift during the Middle Miocene, thereby delaying the age for the onset of subsidence in this region. In the Akitio Basin, the work of Bailleul et al. (2013) supports this result, with a previously established younger subsidence starting at 13.2 Ma. In the Whareama Basin, in the absence of other stratigraphic markers, the age of the MTDs (mid Lillburnian, ca. 14 Ma) can be used as a guide to propose that the subsidence did not start before, at least, 14 Ma. For the Te Wharau Basin, whilst the first recordings of subsidence date from 15 Ma (Chanier et al. 1992; Chanier et al. 1999), periods of active tectonics persisted until the end of the Middle Miocene, particularly affecting the structures to the east (Crundwell 1987). The MTDs spanned the Middle Miocene, Lillburnian and thus cannot be used to precisely refine the age of the generalised subsidence in the Te Wharau Basin. Chanier et al. (1999) observed that this major change in tectonic regime gradually occurred along the margin. We here offer an additional insight as to the subsidence timeframe in the Whareama Basin, shifting the starting age from 15 Ma to 14 Ma at minima.

6.4. Implications for mass-transport deposit nomenclature

Mass-wasting *attached* systems can be divided into two types (Moscardelli and Wood 2008; Moscardelli and Wood 2015). The *shelf-attached* systems are essentially sourced by shelf-edge deltas whose stability is mainly controlled by sea-level changes and sedimentation rates whereas the *slope-attached* systems result from isolated, catastrophic sediment collapse(s) typically related to gas-hydrate dissociation and or tectonic activity (*e.g.,* earthquakes) (Moscardelli and Wood 2008; Moscardelli and Wood 2015). The latter will successfully destabilise huge volumes of sediments simultaneously whereas the former will involve multiple, semi-uninterrupted episodes of mass-failure. As highlighted by Moscardelli and Wood (2015), characterising if a system is *shelf-* or *slope-attached* is particularly critical since it does not only inform on the potential sourcing areas but also helps to better predict the impending causal mechanisms and modalities of development.

Whether or not the shelf-derived MTDs described in this study correspond to the *shelf-attached* or *slope-attached* nomenclature is uncertain. The deposits result from the regional destabilisation of neritic shelfal environments, however there is no evidence of a shelf-edge delta that could have fed such a system in the Hikurangi Margin. In fact, the Hikurangi shelfal environments are often referred to as mixed siliciclastic-carbonate systems formed in association with margin uplift and where the carbonates accumulated on a narrow shelf(ves) receiving recurrent terrigenous input from the hinterland (Caron et al. 2004; Bailleul et al. 2007; Bailleul et al. 2013). As previously discussed, the destabilisation and collapse of these shelfal environments most likely resulted from the generation and destruction of oversteepened slopes controlled by tectonic activity (shortening, uplift and seismicity) rather than changes in eustatic level (see 6.2). The multiple, successive mass-wasting occurrences recorded at outcrop do not point toward an isolated catastrophic event but a series of semi-continuous events with a regional footprint. Similar divergences with such classification have been observed elsewhere in the world in similar tectonically active convergent settings (*e.g.,* in the Sinu fold belt, offshore Colombia (Romero-Otero et al. 2010; Ortiz-Karpf et al. 2018)).

We therefore propose that notwithstanding sea-level changes and high sedimentation rates as causal mechanisms (Posamentier and Walker 2006; Moscardelli and Wood 2008; Moscardelli and Wood 2015; and references within), recurrent tectonic activity (shortening, uplift and related seismicity) along active margins also has potential to trigger large-scale shelf(ves) destabilisation and collapses. Therefore, although these systems, sourced from the shelf, seem to preferentially occur at mature stages of convergent margin development (Underwood and Bachman 1982; Bailleul et al. 2007; Vinnels et al. 2010;

973 Ortiz-Karpf et al. 2018), they will not always post-date the main phases of active tectonics (*i.e.,* can be
974 syn-kinematic) as suggested by Ortiz-Karpf et al. (2018).

975

7. CONCLUSIONS

(1) Sea-level changes and high sedimentation rates are commonly inferred to be the main causal mechanisms for large-scale continental shelf(ves) collapses (*i.e., shelf-attached* systems), thereby underestimating the role of tectonics. This study demonstrates that periods of tectonic activity (shortening, uplift and related seismicity) act as another causal mechanism to consider for large-scale shelf failure. In fact, recurring tectonic motion in compressional settings (*e.g.,* active margins) can not only affect the basin-bounding structures and control the development of the shelfal environments but also drive the recurrent generation and destruction of oversteepened slopes, which can, in turn, favour repeated destabilisation and collapses of the shelves.

(2) Short-lived periods (ca. 1 to 2 Ma) of tectonic activity can result in the emplacement of recurrent mass-wasting products thereby reinforcing the importance of mass-wasting systems in deep-marine fold-and-thrust belt evolution.

(3) Shelf-derived mass-wasting products are preferentially recorded and captured during mature stages of trench-slope basin and subduction margin development. Yet, they do not always post-date the main phases of active tectonics. They can result from the destabilisation and collapses of shelves, either directly attached to the continent or potentially locally isolated, developing upon and about actively fault-growing folds.

(4) The associated shelf-derived products have a regional footprint.

- Both sediment mass-movements (*e.g.,* slides, slumps) and mobilisation (*e.g.,* debris flows) can occur. Yet, cohesive gravity flows dominate, eventually breaking down into a series of erosive, upward fining surges downslope.
- At outcrop scale, the MTDs always incorporate sediments and well-preserved to fragmented macrofossils from neritic shelfal environments and mostly comprise (pre- and syn-kinematic) extraformational clasts. Their sizes generally oscillate between a ten to a couple hundreds of metres (minimum thickness). Regionally extensive, they are

deposited across several intra-slope basins, even though smaller, localized MTDs can also be punctually found.

- At seismic scale, both sediment mass-movements and cohesive gravity flows are commonly observed. However, the seismic resolution does not allow identification of the multitude of downslope surges observed at outcrop-scale. The coalescing gravity flows will be commonly imaged as one single seismofacies, thereby missing the lateral and vertical facies variations. This will, in turn, have a significant impact for both the causal mechanism and stratigraphic predictions.

(5) Taphonomic analysis of the fossil content of MTDs is a powerful tool to gain additional knowledge on the transport and depositional processes of mass-wasting events. It also helps identifying and better characterising the source areas.

(6) Finally, MTDs can be used as a guide to help refining the tectonostratigraphic evolution of subduction complexes and their related trench-slope basins. Here, the analysis of the MTDs allowed us to:

- Reconstruct the depositional systems and palaeogeography at a particular time: the Middle Miocene, Lillburnian not only staged the development of a regional mixed siliciclastic-carbonate shelfal domain across the south-western portion of the Hikurangi Margin but also recorded its coeval destabilisation, which resulted in the remobilisation and deposition of shelf-derived MTDs across several trench-slope basins (*i.e.,* Whareama, Te Wharau and Akitio Basins). The Whareama and Akitio Basins were likely connected at that time (one single trench-slope basin), sharing the same seaward border to the east, controlled by the underlying Whakataki-Turnagain Fault complex to the north, laterally evolving into the Flat Point-Whakataki Fault complex to the south.
- Better characterise the Hikurangi Margin tectonic framework: previous studies have inferred that the margin underwent a major change in tectonic regime at ca. 15 Ma, entering into a period of generalised subsidence. However, this study demonstrates that the southern portion of the Hikurangi Margin was still dominated by shortening and uplift during the Middle Miocene, Lillburnian, and thus, that the subsidence did not start before, at least, ca. 14 Ma in the Whareama Basin.

8. ACKNOWLEDGEMENTS

We thank the Schlumberger HQ teams from London and Oslo, and more particularly Keith Tushingham and Mark Douglas for their initial support four years ago; without their backing, this work would have not been possible. Special thanks to Karen and John Barbour for making us feel like home during our stays at Homewood and for access to the study area. We kindly thank Pierre Malié and Andréa Barrier for their assistance during the fieldwork mission, as well as Romain Armand, François-Xavier Joanny and Pierre Saulet from UniLaSalle (France) for their amazing technical support on the GIS and outcrop modelling workflows. We also thank our colleagues from the Basins-Reservoirs-Resources B2R research unit (University of UniLaSalle, France) and from GNS Science (Lower Hutt, New Zealand) for thoughtful insights and discussions. Finally, we thank the guest-editor Lorna Strachan and Suzanne Bull for their helpful comments and suggestions, this paper also benefiting from feedback from an anonymous reviewer.

9. DISCLOSURE STATEMENT

No potential conflict of interest was reported by the author(s).

10. FUNDING

This research was funded by Schlumberger.

11. DATA AVAILIBILITY STATEMENT

The data that support the findings of this study are openly available in figshare at:

https://figshare.com/articles/journal_contribution/Claussmann_et_al_NZJGG_Supplementary_material/13614101.

1058 # 12. REFERENCES

1059 Allen PA, Dorrell RM, Harlen OG, Thomas RE, McCaffrey WD. 2020. Pulse propagation in gravity
1060 currents. Physics of Fluids. 32(1):016603. https://doi.org/10.1063/1.5130576

1061 Alsop GI, Weinberger R, Marco S, Levi T. 2019. Identifying soft-sediment deformation in rocks. Journal
1062 of Structural Geology. 125:248–255. https://doi.org/10.1016/j.jsg.2017.09.001

1063 Alves TM. 2015. Submarine slide blocks and associated soft-sediment deformation in deep-water basins:
1064 A review. Marine and Petroleum Geology. 67:262–285. https://doi.org/10.1016/j.marpetgeo.2015.05.010

1065 Bailleul J, Caron V, Chanier F, Mahieux G, Malié P, Gagnaison C, Claussmann B, Potel S. Submitted.
1066 Combined tectonic and eustatic controls on the syn-subduction shelfal sedimentation of the Middle
1067 Miocene lower trench-slope of the Hikurangi thrust wedge (North Island, New Zealand). New Zealand
1068 Journal of Geology and Geophysics.

1069 Bailleul J, Chanier F, Ferrière J, Robin C, Nicol A, Mahieux G, Gorini C, Caron V. 2013. Neogene
1070 evolution of lower trench-slope basins and wedge development in the central Hikurangi subduction
1071 margin, New Zealand. Tectonophysics. 591:152–174. https://doi.org/10.1016/j.tecto.2013.01.003

1072 Bailleul J, Robin C, Chanier F, Guillocheau F, Field B, Ferrière J. 2007. Turbidite Systems in the Inner
1073 Forearc Domain of the Hikurangi Convergent Margin (New Zealand): New Constraints on the
1074 Development of Trench-Slope Basins. Journal of Sedimentary Research. 77(4):263–283.
1075 https://doi.org/10.2110/jsr.2007.028

1076 Ballance PF. 1976. Evolution of the Upper Cenozoic Magmatic Arc and plate boundary in northern New
1077 Zealand. Earth and Planetary Science Letters. 28(3):356–370.
1078 https://doi.org/10.1016/0012-821X(76)90197-7

1079 Barnes PM, Ghisetti FC, Ellis S, Morgan JK. 2018. The role of protothrusts in frontal accretion and
1080 accommodation of plate convergence, Hikurangi subduction margin, New Zealand. Geosphere.
1081 14(2):440–468. https://doi.org/10.1130/GES01552.1

1082 Barnes PM, Lamarche G, Bialas J, Henrys S, Pecher I, Netzeband GL, Greinert J, Mountjoy JJ, Pedley
1083 K, Crutchley G. 2010. Tectonic and geological framework for gas hydrates and cold seeps on the
1084 Hikurangi subduction margin, New Zealand. Marine Geology. 272(1–4):26–48.
1085 https://doi.org/10.1016/j.margeo.2009.03.012

1086 Barnes PM, Nicol A, Harrison T. 2002. Late Cenozoic evolution and earthquake potential of an active
1087 listric thrust complex above the Hikurangi subduction zone, New Zealand. GSA Bulletin. 114(11):1379–
1088 1405. https://doi.org/10.1130/0016-7606(2002)114<1379:LCEAEP>2.0.CO;2

1089 Barrier L, Nalpas T, Gapais D, Proust J-N. 2013. Impact of synkinematic sedimentation on the geometry
1090 and dynamics of compressive growth structures: Insights from analogue modelling. Tectonophysics.
1091 608:737–752. https://doi.org/10.1016/j.tecto.2013.08.005

1092 Barton M, O'Byrne C, Pirmez C, Prather BE, van der Vlugt F, Alpak FO, Sylvester Z. 2010. Turbidite
1093 Channel Architecture: Recognizing and Quantifying the Distribution of Channel-base Drapes Using Core
1094 and Dipmetre Data. AAPG Memoir. 92:195–210. https://doi.org/10.1306/13181284M923289

1095 Beavan J, Tregoning P, Bevis M, Kato T, Meertens C. 2002. Motion and rigidity of the Pacific Plate and
1096 implications for plate boundary deformation. Journal of Geophysical Research: Solid Earth.
1097 107(B10):ETG 19-1-ETG 19-15. https://doi.org/10.1029/2001JB000282

1098 Bland KJ, Uruski CI, Isaac MJ. 2015. Pegasus Basin, eastern New Zealand: A stratigraphic record of
1099 subsidence and subduction, ancient and modern. New Zealand Journal of Geology and Geophysics.
1100 58(4):319–343. https://doi.org/10.1080/00288306.2015.1076862

1101 Bradshaw JD. 1989. Cretaceous geotectonic patterns in the New Zealand Region. Tectonics. 8(4):803–
1102 820. https://doi.org/10.1029/TC008i004p00803

1103 Bull S, Browne GH, Arnot MJ, Strachan LJ. 2020. Influence of mass transport deposit (MTD) surface
1104 topography on deep-water deposition: an example from a predominantly fine-grained continental margin,
1105 New Zealand. Geological Society, London, Special Publications. 500(1):147–171.
1106 https://doi.org/10.1144/SP500-2019-192

1107 Bull S, Cartwright J, Huuse M. 2009. A review of kinematic indicators from mass-transport complexes
1108 using 3D seismic data. Marine and Petroleum Geology. 26:1132–1151.

1109 Burgreen B, Graham S. 2014. Evolution of a deep-water lobe system in the Neogene trench-slope setting
1110 of the East Coast Basin, New Zealand: Lobe stratigraphy and architecture in a weakly confined basin
1111 configuration. Marine and Petroleum Geology. 54:1–22. https://doi.org/10.1016/j.marpetgeo.2014.02.011

1112 Cape CD, Lamb SH, Vella P, Wells PE, Woodward DJ. 1990. Geological structure of Wairarapa Valley,
1113 New Zealand, from seismic reflection profiling. Journal of the Royal Society of New Zealand. 20(1):85–
1114 105. https://doi.org/10.1080/03036758.1990.10426734

1115 Carey JM, Crutchley GJ, Mountjoy JJ, Petley DN, McSaveney MJ, Lyndsell B. 2019. Slow episodic
1116 movement driven by elevated pore-fluid pressures in shallow subaqueous slopes. Geomorphology.
1117 329:99–107. https://doi.org/10.1016/j.geomorph.2018.12.034

1118 Caron V. 2011. Contrasted textural and taphonomic properties of high-energy wave deposits cemented
1119 in beachrocks (St. Bartholomew Island, French West Indies). Sedimentary Geology. 237(3):189–208.
1120 https://doi.org/10.1016/j.sedgeo.2011.03.002

1121 Caron V, Bailleul J, Chanier F, Mahieux G. 2021. Episodes of seabed rise and rapid drowning controlling
1122 the development of regressive and transgressive rhodolithic limestones in a tectonically-active
1123 subduction setting (Early Miocene, Wairarapa region, New Zealand). New Zealand Journal of Geology
1124 and Geophysics. https://doi.org/10.1080/00288306.2021.1960865

1125 Caron V, Bailleul J, Chanier F, Mahieux G, Joanny F-X. 2019. A new analytical procedure to graphically
1126 characterise the taphonomic properties of skeletal carbonates. An example from Miocene limestones of
1127 new zealand. PALAIOS. 34(8):364–381. https://doi.org/10.2110/palo.2018.101

1128 Caron V, Nelson CS, Kamp PJJ. 2004. Contrasting carbonate depositional systems for Pliocene cool-
1129 water limestones cropping out in central Hawke's Bay, New Zealand. New Zealand Journal of Geology
1130 and Geophysics. 47(4):697–717. https://doi.org/10.1080/00288306.2004.9515084

1131 Chanier F. 1991. Le prisme d'accrétion Hikurangi : un témoin de l'évolution géodynamique d'une marge
1132 active pacifique (Nouvelle-Zélande) [PhD Thesis]. France: Université de Lille 1.

1133 Chanier F, Ferrière J. 1989. On the existence of major tangential movements in the East Coast Range of
1134 New Zealand: their significance within the framework of Pacific plate subduction. Comptes Rendus de
1135 l'Académie des Sciences - Séries II - Earth and Planetary Science. 308(2):1645–1650.

1136 Chanier F, Ferrière J. 1991. From a passive to an active margin: Tectonic and sedimentary processes
1137 linked to the birth of an accretionary prism (Hikurangi Margin, New Zealand). Société Géologique de
1138 France. 162(4):649–660. https://doi.org/10.2113/gssgfbull.162.4.649

1139 Chanier F, Ferrière J, Angelier J. 1992. Extension and tectonic erosion in an accretionary prism: example
1140 from the Hikurangi Prism, New Zealand. Comptes Rendus de l'Académie des Sciences - Séries IIA -
1141 Earth and Planetary Science. 315(2):741–747.

1142 Chanier F, Ferrière J, Angelier J. 1999. Extensional deformation across an active margin, relations with
1143 subsidence, uplift, and rotations: The Hikurangi subduction, New Zealand. Tectonics. 18(5):862–876.
1144 https://doi.org/10.1029/1999TC900028

1145 Clark K, Howarth J, Litchfield N, Cochran U, Turnbull J, Dowling L, Howell A, Berryman K, Wolfe F. 2019.
1146 Geological evidence for past large earthquakes and tsunamis along the Hikurangi subduction margin,
1147 New Zealand. Marine Geology. 412:139–172. https://doi.org/10.1016/j.margeo.2019.03.004

1148 Couvin B, Georgiopoulou A, Mountjoy JJ, Amy L, Crutchley GJ, Brunet M, Cardona S, Gross F, Böttner
1149 C, Krastel S, Pecher I. 2020. A new depositional model for the Tuaheni Landslide Complex, Hikurangi
1150 Margin, New Zealand. Geological Society, London, Special Publications. 500(1):551–566.
1151 https://doi.org/10.1144/SP500-2019-180

1152 Crundwell M. 1987. Neogene stratigraphy and geological history of the Wainuioru Valley, Eastern
1153 Wairarapa, New Zealand. [BSc Thesis]. Wellington, New Zealand: Victoria University.

1154 Dawson AG, Stewart I. 2007. Tsunami deposits in the geological record. Sedimentary Geology.
1155 200(3):166–183. https://doi.org/10.1016/j.sedgeo.2007.01.002

1156 Einsele G, Chough SK, Shiki T. 1996. Depositional events and their records—an introduction.
1157 Sedimentary Geology. 104(1):1–9. https://doi.org/10.1016/0037-0738(95)00117-4

1158 Felix M, Leszczyński S, Ślączka A, Uchman A, Amy L, Peakall J. 2009. Field expressions of the
1159 transformation of debris flows into turbidity currents, with examples from the Polish Carpathians and the
1160 French Maritime Alps. Marine and Petroleum Geology. 26(10):2011–2020.
1161 https://doi.org/10.1016/j.marpetgeo.2009.02.014

1162 Festa A, Ogata K, Pini GA, Dilek Y, Alonso JL. 2016. Origin and significance of olistostromes in the
1163 evolution of orogenic belts: A global synthesis. Gondwana Research. 39:180–203.
1164 https://doi.org/10.1016/j.gr.2016.08.002

1165 Festa A, Ogata K, Pini GA, Dilek Y, Codegone G. 2015. Late Oligocene–early Miocene olistostromes
1166 (sedimentary mélanges) as tectono-stratigraphic constraints to the geodynamic evolution of the exhumed
1167 Ligurian accretionary complex (Northern Apennines, NW Italy). International Geology Review. 57(5–8):1–
1168 23.

1169 Festa A, Pini GA, Ogata K, Dilek Y. 2019. Diagnostic features and field-criteria in recognition of tectonic,
1170 sedimentary and diapiric mélanges in orogenic belts and exhumed subduction-accretion complexes.
1171 Gondwana Research. 74:7–30. https://doi.org/10.1016/j.gr.2019.01.003

1172 Field B, Uruski CI, Institute of Geological & Nuclear Sciences. 1997. Cretaceous-Cenozoic geology and
1173 petroleum systems of the East Coast region, New Zealand. New Zealand.

1174 Fonnesu M, Patacci M, Haughton PDW, Felletti F, McCaffrey WD. 2016. Hybrid Event Beds Generated
1175 By Local Substrate Delamination On A Confined-Basin Floor. Journal of Sedimentary Research.
1176 86(8):929–943. https://doi.org/10.2110/jsr.2016.58

1177 Frey-Martínez J, Cartwright J, Hall B. 2005. 3D seismic interpretation of slump complexes: examples
1178 from the continental margin of Israel. Basin Research. 17(1):83–108.

1179 Galloway WE. 1998. Siliciclastic Slope and Base-of-Slope Depositional Systems: Component Facies,
1180 Stratigraphic Architecture, and Classification. AAPG Bulletin. 824:569–595.
1181 https://doi.org/10.1306/1D9BC5BB-172D-11D7-8645000102C1865D

1182 Gamberi F, Rovere M, Marani M. 2011. Mass-transport complex evolution in a tectonically active margin
1183 (Gioia Basin, Southeastern Tyrrhenian Sea). Marine Geology. 279(1–4):98–110.
1184 https://doi.org/10.1016/j.margeo.2010.10.015

1185 Graveleau F, Malavieille J, Dominguez S. 2012. Experimental modelling of orogenic wedges: A review.
1186 Tectonophysics. 538–540:1–66. https://doi.org/10.1016/j.tecto.2012.01.027

1187 Hampton MA, Lee HJ, Locat J. 1996. Submarine landslides. Reviews of Geophysics. 34(1):33–59.
1188 https://doi.org/10.1029/95RG03287

1189 Haq BU, Hardenbol J, Vail PR. 1987. Chronology of Fluctuating Sea Levels Since the Triassic. Science.
1190 235(4793):1156–1167. https://doi.org/10.1126/science.235.4793.1156

1191 Henstra GA, Grundvåg S-A, Johannessen EP, Kristensen TB, Midtkandal I, Nystuen JP, Rotevatn A,
1192 Surlyk F, Sæther T, Windelstad J. 2016. Depositional processes and stratigraphic architecture within a
1193 coarse-grained rift-margin turbidite system: The Wollaston Forland Group, east Greenland. Marine and
1194 Petroleum Geology. 76:187–209. https://doi.org/10.1016/j.marpetgeo.2016.05.018

1195 Iverson RM. 1997. The physics of debris flows. Reviews of Geophysics. 35(3):245–296.
1196 https://doi.org/10.1029/97RG00426

1197 Johansen A. 1999. The geology of the upper Tinui Valley, Wairarapa, New Zealand. [BSc Thesis].
1198 Wellington, New Zealand: Victoria University.

1199 Johnson AM. 1984. Debris flow. In: Brunsden D, Prior DB, editors. Slope Instability. New York, America:
1200 Wiley and Sons; p. 257–361.

1201 Jones OT. 1944. The compaction of muddy sediments. Quarterly Journal of the Geological Society.
1202 100(1–4):137–160. https://doi.org/10.1144/GSL.JGS.1944.100.01-04.09

1203 Karig DE, Moore GF, Curray JR, Lawrence MB. 1980. Morphology and shallow structure of the lower
1204 trench slope off Nias Island, Sunda Arc. In: Hayes DE, editor. The Tectonic and Geologic Evolution of
1205 Southeast Asian Seas and Islands. Washington, America; p. 179–208.

1206 Kidwell SM. 1989. Stratigraphic Condensation of Marine Transgressive Records: Origin of Major Shell
1207 Deposits in the Miocene of Maryland. The Journal of Geology. 97(1):1–24.

1208 Kneller B. 1995. Beyond the turbidite paradigm: physical models for deposition of turbidites and their
1209 implications for reservoir prediction. Geological Society, London, Special Publications. 94(1):31–49.
1210 https://doi.org/10.1144/GSL.SP.1995.094.01.04

1211 Kneller B, McCaffrey W. 1999. Depositional effects of flow nonuniformity and stratification within turbidity
1212 currents approaching a bounding slope; deflection, reflection, and facies variation. Journal of
1213 Sedimentary Research. 69(5):980–991. https://doi.org/10.2110/jsr.69.980

1214 Kuenen PhH. 1964. Deep-Sea Sands and Ancient Turbidites. In: Bouma AH, Brouwer A, editors.
1215 Developments in Sedimentology. Vol. 3. Netherlands: Elsevier; p. 3–33. https://doi.org/10.1016/S0070-
1216 4571(08)70953-1

1217 Lamarche G, Joanne C, Collot J-Y. 2008. Successive, large mass-transport deposits in the south
1218 Kermadec fore-arc basin, New Zealand: The Matakaoa Submarine Instability Complex. Geochemistry,
1219 Geophysics, Geosystems. 9(4):1–30. https://doi.org/10.1029/2007GC001843

1220 Lamb SH, Vella P. 1987. The last million years of deformation in part of the New Zealand plateboundary
1221 zone. Journal of Structural Geology. 9(7):877–891. https://doi.org/10.1016/0191-8141(87)90088-5

1222 Lee HJ. 2009. Timing of occurrence of large submarine landslides on the Atlantic Ocean margin. Marine
1223 Geology. 264(1–2):53–64. https://doi.org/10.1016/j.margeo.2008.09.009

1224 Lee J, Begg J. 2002. Geology of the Wairarapa area. Institute of Geological & Nuclear Sciences 1:250
1225 000 geological map: Institute of Geological & Nuclear Sciences Limited.

1226 Lehu R, Lallemand S, Hsu S-K, Babonneau N, Ratzov G, Lin AT, Dezileau L. 2015. Deep-sea
1227 sedimentation offshore eastern Taiwan: Facies and processes characterisation. Marine Geology. 369:1–
1228 18. https://doi.org/10.1016/j.margeo.2015.05.013

1229 Lewis KB, Barnes PM, Garlick RD. 1999. Central Hikurangi GeodyNZ swath maps: depths, texture and
1230 geological interpretation.

1231 Lewis KB, Lallemand SE, Carter L. 2004. Collapse in a Quaternary shelf basin off East Cape, New
1232 Zealand: Evidence for passage of a subducted seamount inboard of the Ruatoria giant avalanche. New
1233 Zealand Journal of Geology and Geophysics. 47(3):415–429.
1234 https://doi.org/10.1080/00288306.2004.9515067

1235 Lewis KB, Pettinga JR. 1993. The emerging, imbricate frontal wedge of the Hikurangi margin. In: Ballance
1236 PF, editor. South Pacific sedimentary basins. Amsterdam, Netherlands: Elsevier Science; p. 225–250.

1237 Li KM, Zuo L, Nardelli V, Alves TM, Lourenço SDN. 2019. Morphometric signature of sediment particles
1238 reveals the source and emplacement mechanisms of submarine landslides. Landslides. 16(4):829–837.
1239 https://doi.org/10.1007/s10346-018-01123-1

1240 Lowe DR. 1982. Sediment gravity flows; II, Depositional models with special reference to the deposits of
1241 high-density turbidity currents. Journal of Sedimentary Research. 52(1):279–297.
1242 https://doi.org/10.1306/212F7F31-2B24-11D7-8648000102C1865D

1243 Malavieille J. 2010. Impact of erosion, sedimentation, and structural heritage on the structure and
1244 kinematics of orogenic wedges: Analog models and case studies. GSAT. 20(1):4–10.
1245 https://doi.org/10.1130/GSATG48A.1

Malie P, Bailleul J, Chanier F, Toullec R, Mahieux G, Caron V, Field B, Mählmann RF, Potel S. 2017. Spatial distribution and tectonic framework of fossil tubular concretions as onshore analogues of cold seep plumbing systems, North Island of New Zealand. Bulletin de la Société géologique de France. 188(4):25. https://doi.org/10.1051/bsgf/2017192

Martin RE. 1999. Taphonomy: A Process Approach. Cambridge, United Kingdom: Cambridge University Press. https://doi.org/10.1017/CBO9780511612381

McArthur AD, Bailleul J, Mahieux G, Claussmann B, Wunderlich A, McCaffrey WD. 2021. Deformation-sedimentation feedback and the development of anomalously thick aggradational turbidite lobes: subsurface and outcrop examples from the Hikurangi Margin, New Zealand. Journal of Sedimentary Research. 91(4):362–389. https://doi.org/10.2110/jsr.2020.013

McArthur AD, Claussmann B, Bailleul J, McCaffrey W, Clare A. 2019. Variation in syn-subduction sedimentation patterns from inner to outer portions of deep-water fold and thrust belts: examples from the Hikurangi subduction margin of New Zealand. Geological Society, London, Special Publications. 490:285–310. https://doi.org/10.1144/SP490-2018-95

McArthur AD, Jolley DW, Hartley AJ, Archer SG, Lawrence HM. 2016. Palaeoecology of syn-rift topography: A Late Jurassic footwall island on the Josephine Ridge, Central Graben, North Sea. Palaeogeogr Palaeoclimatol Palaeoecol. 459:63–75. https://doi.org/10.1016/j.palaeo.2016.06.033

McArthur AD, McCaffrey WD. 2019. Sedimentary architecture of detached deep-marine canyons: Examples from the East Coast Basin of New Zealand. Sedimentology. 66(3):1067–1101. https://doi.org/10.1111/sed.12536

McHargue T, Pyrcz MJ, Sullivan MD, Clark JD, Fildani A, Romans BW, Covault JA, Levy M, Posamentier HW, Drinkwater NJ. 2011. Architecture of turbidite channel systems on the continental slope: Patterns and predictions. Marine and Petroleum Geology. 28(3):728–743. https://doi.org/10.1016/j.marpetgeo.2010.07.008

Middleton GV, Hampton MA. 1973. Sediment Gravity Flows: Mechanics of Flow and Deposition. In: Middleton GV, Bouma AH, editors. Turbidites and Deep-Water Sedimentation. Society of Economic Paleontologists and Mineralogists Pacific Section Short Course; p. 1–38.

Miller KG, Kominz MA, Browning JV, Wright JD, Mountain GS, Katz ME, Sugarman PJ, Cramer BS, Christie-Blick N, Pekar SF. 2005. The Phanerozoic record of global sea-level change. Science. 310(5752):1293–1298. https://doi.org/10.1126/science.1116412

Mohrig D, Ellis C, Parker G, Whipple KX, Hondzo M. 1998. Hydroplaning of subaqueous debris flows. GSA Bulletin. 110(3):387–394. https://doi.org/10.1130/0016-7606(1998)110<0387:HOSDF>2.3.CO;2

Moore GF, Aung LT, Fukuchi R, Sample JC, Hellebrand E, Kopf A, Naing W, Than WM, Tun TN. 2019. Tectonic, diapiric and sedimentary chaotic rocks of the Rakhine coast, western Myanmar. Gondwana Research. 74:126–143. https://doi.org/10.1016/j.gr.2019.04.006

Moore GF, Karig DE. 1976. Development of sedimentary basins on the lower trench slope. Geology. 4(11):693–697. https://doi.org/10.1130/0091-7613(1976)4<693:DOSBOT>2.0.CO;2

Mortimer N. 2004. New Zealand's Geological Foundations. Gondwana Research. 7(1):261–272. https://doi.org/10.1016/S1342-937X(05)70324-5

1285 Moscardelli L, Wood L. 2008. New classification system for mass transport complexes in offshore
1286 Trinidad. Basin Research. 20(1):73–98. https://doi.org/10.1111/j.1365-2117.2007.00340.x

1287 Moscardelli L, Wood L. 2015. Morphometry of mass-transport deposits as a predictive tool. GSA Bulletin.
1288 128(1–2):47–80.

1289 Moscardelli LG, Wood LJ, Mann PC. 2006. Mass-transport complexes and associated processes in the
1290 offshore area of Trinidad and Venezuela. AAPG Bulletin. 90(7):1059–1088.
1291 https://doi.org/10.1306/02210605052

1292 Mulder T, Alexander J. 2001. The physical character of subaqueous sedimentary density flows and their
1293 deposits. Sedimentology. 48(2):269–299. https://doi.org/10.1046/j.1365-3091.2001.00360.x

1294 Mulder T, Cochonat P. 1996. Classification of offshore mass movements. Journal of Sedimentary
1295 Research. 66(1):43–57. https://doi.org/10.1306/D42682AC-2B26-11D7-8648000102C1865D

1296 Mulder T, Syvitski JPM, Migeon S, Faugères J-C, Savoye B. 2003. Marine hyperpycnal flows: initiation,
1297 behavior and related deposits. A review. Marine and Petroleum Geology. 20(6):861–882.
1298 https://doi.org/10.1016/j.marpetgeo.2003.01.003

1299 Naranjo-Vesga J, Ortiz-Karpf A, Wood L, Jobe Z, Paniagua-Arroyave JF, Shumaker L, Mateus-Tarazona
1300 D, Galindo P. 2020. Regional controls in the distribution and morphometry of deep-water gravitational
1301 deposits along a convergent tectonic margin. Southern Caribbean of Colombia. Marine and Petroleum
1302 Geology. 121:104639. https://doi.org/10.1016/j.marpetgeo.2020.104639

1303 Nardin TR, Hein FJ, Gorsline DS, Edwards BD. 1979. A review of mass movement processes, sediment
1304 and acoustic characteristics, and contrasts in slope and base-of-slope systems versus canyon-fan-basin
1305 floor systems. SEPM Special Publication. 27:61–73.

1306 Neef G. 1992. Geology of the Akitio area (1:50 000 metric sheet U25BD, east), northeastern Wairarapa,
1307 New Zealand. New Zealand Journal of Geology and Geophysics. 35(4):533–548.
1308 https://doi.org/10.1080/00288306.1992.9514546

1309 Neef G. 1999. Neogene development of the onland part of the forearc in northern Wairarapa, North Island,
1310 New Zealand: A synthesis. New Zealand Journal of Geology and Geophysics. 42(1):113–135.
1311 https://doi.org/10.1080/00288306.1999.9514835

1312 Nelson CH, Escutia C, Damuth JE, Cushman Twichell D. 2011. Interplay of Mass-Transport and
1313 Turbidite-System Deposits in Different Active Tectonic and Passive Continental Margin Settings: External
1314 and Local Controlling Factors. In: Shipp RC, Weimer P, Posamentier HW, editors. Mass-Transport
1315 Deposits in Deepwater Settings. Oklahoma, America: SEPM; p. 39–68.

1316 Nemec W. 1990. Aspects of Sediment Movement on Steep Delta Slopes. In: Collela A, Prior DB, editors.
1317 Coarse-Grained Deltas. Oxford, United Kingdom: John Wiley & Sons, Ltd; p. 29–73.
1318 https://doi.org/10.1002/9781444303858.ch3

1319 Nemec W, Steel RJ. 1984. Alluvial and Coastal Conglomerates: Their Significant Features and Some
1320 Comments on Gravelly Mass-Flow Deposits. In: Koster EH, Steel RJ, editors. Sedimentology of Gravels
1321 and Conglomerates, Memoir 10. Canada: Canadian Society of Petroleum Geologists; p. 1–31.

1322 Nicol A, Mazengarb C, Chanier F, Rait G, Uruski C, Wallace L. 2007. Tectonic evolution of the active
1323 Hikurangi subduction margin, New Zealand, since the Oligocene. Tectonics. 26(4):1–24.

https://doi.org/10.1029/2006TC002090

Nicol A, VanDissen R, Vella P, Alloway B, Melhuish A. 2002. Growth of contractional structures during the last 10 m.y. at the southern end of the emergent Hikurangi forearc basin, New Zealand. New Zealand Journal of Geology and Geophysics. 45(3):365–385. https://doi.org/10.1080/00288306.2002.9514979

Noda A. 2018. Forearc Basin Stratigraphy and Interactions With Accretionary Wedge Growth According to the Critical Taper Concept. Tectonics. 37(3):965–988. https://doi.org/10.1002/2017TC004744

Ogata K, Festa A, Pini GA, Alonso JL. 2019. Submarine Landslide Deposits in Orogenic Belts: Olistostromes and Sédimentary Mélanges. In: Ogata K, Festa A, Pini GA, editors. Submarine Landslides: Subaqueous Mass Transport Deposits from Outcrops to Seismic Profiles. America: American Geophysical Union (AGU); p. 1–26. https://doi.org/10.1002/9781119500513.ch1

Ogata K, Pogačnik Ž, Pini GA, Tunis G, Festa A, Camerlenghi A, Rebesco M. 2014. The carbonate mass transport deposits of the Paleogene Friuli Basin (Italy/Slovenia): Internal anatomy and inferred genetic processes. Marine Geology. 356:88–110. https://doi.org/10.1016/j.margeo.2014.06.014

Ortiz-Karpf A, Hodgson DM, Jackson CA-L, McCaffrey WD. 2018. Mass-transport complexes as markers of deep-water fold-and-thrust belt evolution: insights from the southern Magdalena fan, offshore Colombia. Basin Research. 30(S1):65–88. https://doi.org/10.1111/bre.12208

Perry CT. 1998. Grain susceptibility to the effects of microboring: implications for the preservation of skeletal carbonates. Sedimentology. 45(1):39–51. https://doi.org/10.1046/j.1365-3091.1998.00134.x

Pettinga JR. 1982. Upper Cenozoic structural history, coastal Southern Hawke's Bay, New Zealand. New Zealand Journal of Geology and Geophysics. 25(2):149–191. https://doi.org/10.1080/00288306.1982.10421407

Pickering KT, Corregidor J. 2005. Mass transport complexes and tectonic control on confined basin-floor submarine fans, Middle Eocene, south Spanish Pyrenees. Geological Society, London, Special Publications. 244(1):51–74. https://doi.org/10.1144/GSL.SP.2005.244.01.04

Pierson TC. 1981. Dominant particle support mechanisms in debris flows at Mt Thomas, New Zealand, and implications for flow mobility. Sedimentology. 28(1):49–60. https://doi.org/10.1111/j.1365-3091.1981.tb01662.x

Pilarczyk JE, Dura T, Horton BP, Engelhart SE, Kemp AC, Sawai Y. 2014. Microfossils from coastal environments as indicators of paleo-earthquakes, tsunamis and storms. Palaeogeography, Palaeoclimatology, Palaeoecology. 413:144–157. https://doi.org/10.1016/j.palaeo.2014.06.033

Posamentier HW, Allen GP, editors. 1999. Siliciclastic Sequence Stratigraphy - Concepts and Applications. Oklahoma, America: SEPM Society for Sedimentary Geology.

Posamentier HW, Kolla V. 2003. Seismic geomorphology and stratigraphy of depositional elements in deep-water settings. Journal of Sedimentary Research. 73(3):367–388.

Posamentier HW, Martinsen OJ. 2011. The Character and Genesis of Submarine Mass-Transport Deposits: Insights from Outcrop and 3D Seismic Data. In: Shipp RC, Weimer P, Posamentier HW, editors. Mass-Transport Deposits in Deepwater Settings. Oklahoma, America: SEPM; p. 7–38.

Posamentier HW, Walker RG. 2006. Deep-Water Turbidites and Submarine Fans. In: Posamentier HW, Walker RG, editors. Facies Models Revisited. Oklahoma, America: SEPM Special Publication 84; p. 397–520. https://doi.org/10.2110/pec.06.84

Postma G, Nemec W, Kleinspehn KL. 1988. Large floating clasts in turbidites: a mechanism for their emplacement. Sedimentary Geology. 58(1):47–61. https://doi.org/10.1016/0037-0738(88)90005-X

Prélat A, Hodgson DM, Flint SS. 2009. Evolution, architecture and hierarchy of distributary deep-water deposits: a high-resolution outcrop investigation from the Permian Karoo Basin, South Africa. Sedimentology. 56(7):2132–2154. https://doi.org/10.1111/j.1365-3091.2009.01073.x

Raine JI, Beu A, Boyes A, Campbell H, Cooper R, Crampton J, Crundwell M, Hollis C, Morgans H, Mortimer N. 2015. New Zealand Geological Timescale NZGT 2015/1. New Zealand Journal of Geology and Geophysics. 58(4):398–403. https://doi.org/10.1080/00288306.2015.1086391

Rait G, Chanier F, Waters DW. 1991. Landward- and seaward-directed thrusting accompanying the onset of subduction beneath New Zealand. Geology. 19(3):230–233. https://doi.org/10.1130/0091-7613(1991)019<0230:LASDTA>2.3.CO;2

Raymond LA. 2019. Perspectives on the roles of melanges in subduction accretionary complexes: A review. Gondwana Research. 74:68–89. https://doi.org/10.1016/j.gr.2019.03.005

Reagan MT, Moridis GJ. 2008. Dynamic response of oceanic hydrate deposits to ocean temperature change. Journal of Geophysical Research: Oceans. 113(C12):1–21. https://doi.org/10.1029/2008JC004938

Richet R, Chazottes V, Cabioch G, Frank N, S. Burr G. 2011. Microborer ichnocoenoses in Quaternary corals from New Caledonia: reconstructions of paleo-water depths and reef growth strategies in relation to environmental changes. Quaternary Science Reviews. 30(19):2827–2838. https://doi.org/10.1016/j.quascirev.2011.06.019

Romero-Otero GA, Slatt RM, Pirmez C. 2010. Detached and Shelf-Attached Mass Transport Complexes on the Magdalena Deepwater Fan. In: Mosher DC, Shipp RC, Moscardelli L, Chaytor JD, Baxter CDP, Lee HJ, Urgeles R, editors. Submarine Mass Movements and Their Consequences. Dordrecht, Netherlands: Springer Netherlands; p. 593–606. https://doi.org/10.1007/978-90-481-3071-9_48

Schlager W, Camber O. 1986. Submarine slope angles, drowning unconformities, and self-erosion of limestone escarpments. Geology. 14(9):762–765. https://doi.org/10.1130/0091-7613(1986)14<762:SSADUA>2.0.CO;2

Sobiesiak MS, Kneller B, Alsop GI, Milana JP. 2018. Styles of basal interaction beneath mass transport deposits. Marine and Petroleum Geology. 98:629–639. https://doi.org/10.1016/j.marpetgeo.2018.08.028

Spörli KB. 1980. New Zealand and Oblique-Slip Margins: Tectonic Development up to and during the Cainozoic. In: Ballance PF, Reading HG, editors. Sedimentation in Oblique-Slip Mobile Zones. United Kingdom: John Wiley & Sons, Ltd; p. 147–170. https://doi.org/10.1002/9781444303735.ch9

Storti F, McClay K. 1995. Influence of syntectonic sedimentation on thrust wedges in analogue models. Geology. 23(11):999–1002. https://doi.org/10.1130/0091-7613(1995)023<0999:IOSSOT>2.3.CO;2

Stow DAV. 1986. Deep clastic seas. In: Reading HG, editor. Sedimentary Environments and Facies. 2nd edition. Oxford, United Kingdom: Blackwell Scientific Publications; p. 399–444.

1400 Strachan LJ. 2008. Flow transformations in slumps: a case study from the Waitemata Basin, New
1401 Zealand. Sedimentology. 55(5):1311–1332. https://doi.org/10.1111/j.1365-3091.2007.00947.x

1402 Strasser M, Moore GF, Kimura G, Kopf AJ, Underwood MB, Guo J, Screaton EJ. 2011. Slumping and
1403 mass transport deposition in the Nankai fore arc: Evidence from IODP drilling and 3-D reflection seismic
1404 data. Geochemistry, Geophysics, Geosystems. 12(5):1–24. https://doi.org/10.1029/2010GC003431

1405 Talling PJ, Masson DG, Sumner EJ, Malgesini G. 2012. Subaqueous sediment density flows:
1406 Depositional processes and deposit types. Sedimentology. 59(7):1937–2003.
1407 https://doi.org/10.1111/j.1365-3091.2012.01353.x

1408 Underwood M, Moore G, Taira A, Klaus A, Wilson M, Fergusson C, Hirano S, Steurer J. 2003.
1409 Sedimentary and Tectonic Evolution of a Trench-Slope Basin in the Nankai Subduction Zone of
1410 Southwest Japan. Journal of Sedimentary Research. 73:589–602.
1411 https://doi.org/10.1306/092002730589

1412 Underwood MB, Bachman SB. 1982. Sedimentary facies associations within subduction complexes.
1413 Geological Society, London, Special Publications. 10(1):537–550.
1414 https://doi.org/10.1144/GSL.SP.1982.010.01.35

1415 Underwood MB, Moore GF. 1995. Trenches and trench-slope basins. In: Busby CJ, Ingersoll RV, editors.
1416 Tectonics of sedimentary basins. Oxford, United Kingdom: Blackwell Science; p. 179–219.

1417 Urgeles R, Camerlenghi A. 2013. Submarine landslides of the Mediterranean Sea: Trigger mechanisms,
1418 dynamics, and frequency-magnitude distribution. Journal of Geophysical Research: Earth Surface.
1419 118(4):2600–2618. https://doi.org/10.1002/2013JF002720

1420 Urlaub M, Talling PJ, Masson DG. 2013. Timing and frequency of large submarine landslides:
1421 implications for understanding triggers and future geohazard. Quaternary Science Reviews. 72:63–82.
1422 https://doi.org/10.1016/j.quascirev.2013.04.020

1423 Vinnels JS, Butler RWH, McCaffrey WD, Paton DA. 2010. Depositional processes across the Sinú
1424 Accretionary Prism, offshore Colombia. Marine and Petroleum Geology. 27(4):794–809.
1425 https://doi.org/10.1016/j.marpetgeo.2009.12.008

1426 Watson SJ, Mountjoy JJ, Crutchley GJ. 2020. Tectonic and geomorphic controls on the distribution of
1427 submarine landslides across active and passive margins, eastern New Zealand. Geological Society,
1428 London, Special Publications. 500:477–494. https://doi.org/10.1144/SP500-2019-165

1429 Westoby MJ, Brasington J, Glasser NF, Hambrey MJ, Reynolds JM. 2012. 'Structure-from-Motion'
1430 photogrammetry: A low-cost, effective tool for geoscience applications. Geomorphology. 179:300–314.
1431 https://doi.org/10.1016/j.geomorph.2012.08.021

1432 Woodcock NH. 1979. The use of slump structures as palaeoslope orientation estimators. Sedimentology.
1433 26(1):83–99. https://doi.org/10.1111/j.1365-3091.1979.tb00339.x

1434 Zanuttigh B, Lamberti A. 2007. Instability and surge development in debris flows. Reviews of Geophysics.
1435 45(3). https://doi.org/10.1029/2005RG000175

1436 Zuschin M, Stachowitsch M, Stanton RJ. 2003. Patterns and processes of shell fragmentation in modern
1437 and ancient marine environments. Earth-Science Reviews. 63(1):33–82. https://doi.org/10.1016/S0012-
1438 8252(03)00014-X

13. FIGURES

Figure 1: Generic model for trench-slope systems. Evolving structural style towards the trench influences the generation of accommodation space and sediment pathways. (g): Failure of the regional continental shelf and upper-slope regions will source attached mass-wasting systems (*sensu* Moscardelli and Wood 2008) and thus large-scale mass-transport deposits. (h): Collapse of the local thrust-related slopes will feed detached systems (*sensu* Moscardelli and Wood 2008), characterised by smaller, localized mass-transport deposits. Modified from McArthur et al. (2019).

Figure 2: (A): Plate tectonic setting of New Zealand. (B): Major subduction-related morphostructural features of the Hikurangi Margin. Black arrows show present-day relative plate motion between the Pacific and Australian plates from Beavan et al. (2002). See (C) for the a – b general cross-section of the Hikurangi subduction complex. (C.R – Coastal Ranges). Modified after Chanier et al. (1999); Bailleul et al. (2007, 2013).

Figure 3: Bathymetric map (Lewis et al. 1999) and onshore structural map (modified from Chanier et al. (1999), Lee and Begg (2002) and Bailleul et al. (2013)) of the southern Hikurangi subduction wedge. The offshore area includes the location of the well Titihaoa-1. Locations of the fault complexes = (I): Adams-Tinui Fault complex, (II): Pukeroro Fault, (III): Flat Point-Whakataki Fault complex to the south, evolving into the Whakataki-Turnagain Fault complex to the north, (IV): Turnagain Fault from Malie et al. (2017). Location of the onshore sedimentological vertical sections displaying Middle Miocene [NZ stage: Lillburnian] shelfal deposits = (f): Fingerpost section, (m): Waihoki-Mangatiti section, (p): Pongaroa section, (t): Takiritini section from Bailleul et al. (2013) and Caron et al. (2019); (ms) : Mapapa stream section from Chanier (1991); (i): Tinui section from Johansen (1999) and Bailleul et al. (2013); (w): Wainuioru sections from Crundwell (1987) and Chanier (1991) and late Middle Miocence [NZ stage: Waiauan] shelfal deposits = (o): Oumukura section from Chanier (1991). Location of the onshore sedimentological vertical sections displaying Middle Miocene [NZ stage: Lillburnian] MTDs = (b): Branscombe section from Bailleul et al. (2013); (tw): Te Wharau road sections; (n): Ngaumu section, (r): Rangiora section; (s): Sefton Hills sections; (c): Craigie Lea section.

Figure 4: Chronostratigraphic chart for the southern emerged portion of the Hikurangi subduction wedge. Lithostratigraphy details adapted from Chanier (1991), Chanier and Ferrière (1991), Field et al. (1997), Lee and Begg (2002) and Bland et al. (2015); and detailing the pre- and syn-Hikurangi subduction series. Regional tectonism adapted from Chanier et al. (1999), Bailleul et al. (2013) and Malie et al. (2017). New Zealand stages after Raine et al. (2015) showing the equivalence with the international stages.

Figure 5: Satellite map from World Imagery (ESRI), and onshore geological map from Chanier (1991) of the Te Wharau and Whareama Basin areas. Location of the drone acquisition and related 3D outcrop model = (s-1): Sefton Hills section. Location of the onshore sedimentological vertical sections displaying Middle Miocene [NZ stage: Lillburnian] shelfal deposits = (ms): Mapapa stream section from Chanier (1991), (w): Wainuioru sections from Crundwell (1987) and Chanier (1991) and late Middle Miocene [NZ stage stage: Waiauan] shelfal deposits = (o): Oumukura section from Chanier (1991). Location of the onshore sedimentological vertical sections displaying Middle Miocene [NZ stage stage: Lillburnian] MTDs = (c): Craigie Lea section, (n): Ngaumu section, (r): Rangiora section, (s-1, s-2): Sefton Hills sections, (tw-1, tw-2): Te Wharau road sections.

Figure 6: 3D outcrop model (top) and interpretation (bottom) of the Sefton Hills coastal outcrop (section-1). The letters refer to some of the architectural elements that supported the interpretations and which are detailed in Figure 8 and Figure 9. Stereoplots (Schmidt, lower hemisphere) highlight the palaeocurrents measured in the turbidites (Fa1g) as well as the fold axis and planes of the slump-related folds measured in the shelf-derived mass-transport deposits (Fa3p) after back-tilting of bedding planes to initial horizontal position (assuming cylindrical folding).

Figure 7: Sedimentary section 01 (SS-01) recorded at the Sefton Hills outcrop locality (section s-1). Location is found on Figure 6. This section covers the upper part of the turbidite system and ends at the top of the first mass-wasting event which comprises three distinct lithofacies (DF, MF-1, MF-2, see Table 1). Details on the facies assemblages (FA) are provided in Table 1. All the palaeocurrent and slump measurements were taken along this section, respectively in the turbidites (Fa1g) and mass-transport deposits (Fa3p).

Figure 8: Detailed views of the turbidite system's main architectural and sedimentary elements supporting the interpretation of the Sefton Hills 3D outcrop model (Figure 6). (a, b, g, h): thick to thin-bedded turbidites (Fa1g-c to Fa1g-a), comprising low-angle, concave-up, elongated bodies, sometimes slightly eroding into a basal mud drape and either showing fining and thinning upward trend or a simple mudstone cap; (a, d, e): contorted and dislocated turbidites between undeformed strata (Fa3l-s); (c, d): example of very thin- to medium-bedded turbidites from Fa1g-f; (e, f): example of sheet-like turbidites from Fa1s; (h): intra-turbidite debris flow mostly made of dislocated turbidites and some rare floating bioclasts (Fa3l-d).

Figure 9: Detailed views of the shelf-derived mass-transport deposits (MTDs) main architectural and sedimentary elements supporting the interpretation of the Sefton Hills 3D outcrop model (Figure 6). (a, b, c, e, h): sharp, slightly erosional bases between distinct MTDs; (a): pluri-decametric turbidite raft incorporated in lithofacies MF-1 (second occurrence, MF-1b); (b, e): decametric mud clasts in lithofacies DF (second occurrence, DFb); (c): increasing mud clast content toward the top of lithofacies DF (first occurrence, DFa); (d): contorted thin-bedded turbidites in MF-2 (second occurrence, MF-2b); (f): overturned turbidite rafts and stratigraphic, locally structurally-controlled, contact between the MTDs and underlying turbidite system; (g): lateral continuity of the lithofacies MF-2 which can be traced over one kilometre to the south (Sefton Hills section s-2).

Figure 10: Detailed description of the three main lithofacies (DF, MF-1 and MF-2) resulting from mass-wasting events that reworked shelf-derived material. Descriptions mainly summarise the observations made at the Sefton Hills locality (Whareama Basin) (Figure 6; Figure 7; Figure 9). Insights from the inland outcrops (Te Wharau Basin) were also incorporated. (a, h, n): matrix; (b, c, d, e, i, j, k, o): syn-subduction lithoclasts, *e.g.,* turbidites, mud clasts, shell bed clasts; (f, l): pre-subduction lithoclasts; (g, m): syn-subduction bioclasts, *i.e.,* skeletons from neritic faunal assemblages. Details in Table 1.

Figure 11: Detailed views of Te Wharau Basin shelf-derived mass-transport deposits. (a): hinterland outcrop conditions, gravel-grade extraformational clasts within a silty mudstone matrix; (b): sub-angular cobble of shell bed clast and granules to pebbles of pre-subduction-dominated lithoclasts; (c): cobbles and boulders of pre- (*e.g.,* Torlesse material) and syn-subduction (*e.g.,* shell beds) lithoclasts; (d): chalky molluscan skeletons and lithoclasts from (predominantly) pre-subduction strata floating in a silty mudstone matrix; (e): outsized clast of bioclastic fine-grained sandstones from middle to outer shelf environments; (f): granules to cobbles of pre-subduction material that includes small, sub-rounded pebbles of already reworked Torlesse greywackes.

Figure 12: Taphonomic characterisation of fossil remains described from 1x1 m area of outcrop at three different localities, using frequency histograms of the degree of alteration (e.g., low, moderate, high) for each category of skeleton damage (i.e., fragmentation, abrasion, bioerosion) and encrustation. Lithofacies DF and MF-1 are described in details in Figure 10. Note that data for lithofacies MF-1 are only available for the finest skeletal fraction, coarser material being rare (n=3). Photographs of fossil remains illustrate the qualitative grading evaluation of taphonomic features in the field. Arrows in photographs 3 and 4 point to bio-erosional features. Arrows in photographs 5 and 6 point to the analysed bioclasts. Scales in cm.

Figure 13: Depositional processes and stratigraphic record of shelf-derived mass-wasting event at outcrop scale. Shelf failure will trigger both: (1) sediment mass-failure and mobilisation close to the source region(s), on the slope and (2) cohesive gravity flow deposition onto the basin floor: either as a single cohesive flow or eventually breaking down into a series of erosive, upward fining surges downslope. The wide range of lithofacies always incorporates reworked well-preserved to fragmented macrofaunal assemblages from neritic shelfal environments. They will also include extraformational clasts either (1) originating from the failed source area, (2) incorporated during the transport downslope and or (3) resulting from the partial destabilisation of the substratum upon which the shelfal environment was settling.

Figure 14: Area vs length log-log plot showcasing the morphometric parameter values calculated for the mass-transport deposits (MTDs) described in this study using the sets of equations from Moscardelli and Wood (2015). See Appendix 4 for details on the equations, calculations and associated results for each of the occurrences. Whether using the general or specific set of equations, two main families of MTDs were identified using the nomenclature from Moscardelli and Wood (2015): (1) the Te Wharau Basin shelf-derived MTDs are best regrouped under the detached systems whereas (2) the Akitio and Whareama Basin shelf-derived MTDs under the attached systems.

Figure 15: Periods of repeated tectonic activity at basin-bounding structures will not only result in the development of neritic conditions and settlement of related faunal assemblages at shallow waters, but also favour the expansion of abrupt, unstable areas close to the shelf-margins installed above the thrust forelimb. The recurring generation and destruction of oversteepened slopes will in turn favour the repeated destabilisation and collapses of the shelves.

Figure 16: Schematic palaeogeographic map of the south-western portion of the Hikurangi Margin (Coastal Ranges) during the Lillburnian. This period not only staged the development of regional shelfal domain(s) (Crundwell 1987; Chanier 1991; Bailleul et al. 2007; Bailleul et al. 2013) but also recorded their concomitant destabilisation and failure(s). This(these) resulted in the emplacement of a multitude of MTDs, occluding the previously developing systems, such as the Sefton Hills turbidite systems in the Whareama Basin or the Kings canyon system (see McArthur and McCaffrey (2019) in the Akitio Basin. The development of the shelves occurred above substantially different substratum inherited from local tectonics, thereby allowing through the analysis of the reworked material to retrace the potential sourcing region(s) of the different MTDs (*e.g.,* southern and northern shelfal domains). See Figure 3 for the name of the shelfal and MTD outcrops.

Table 1: Characteristics and interpretation of the sedimentary facies for the turbidite systems (Fa1) and mass-wasting systems (Fa3) observed in the study area, mostly from the Sefton Hills outcrop (Whareama basin). The nomenclature is based upon the initial classification defined by Bailleul et al. (2007) and Bailleul et al. (2013). Pictures of the facies associations can be found in Figure 8, Figure 9, Figure 10; Figure 11.

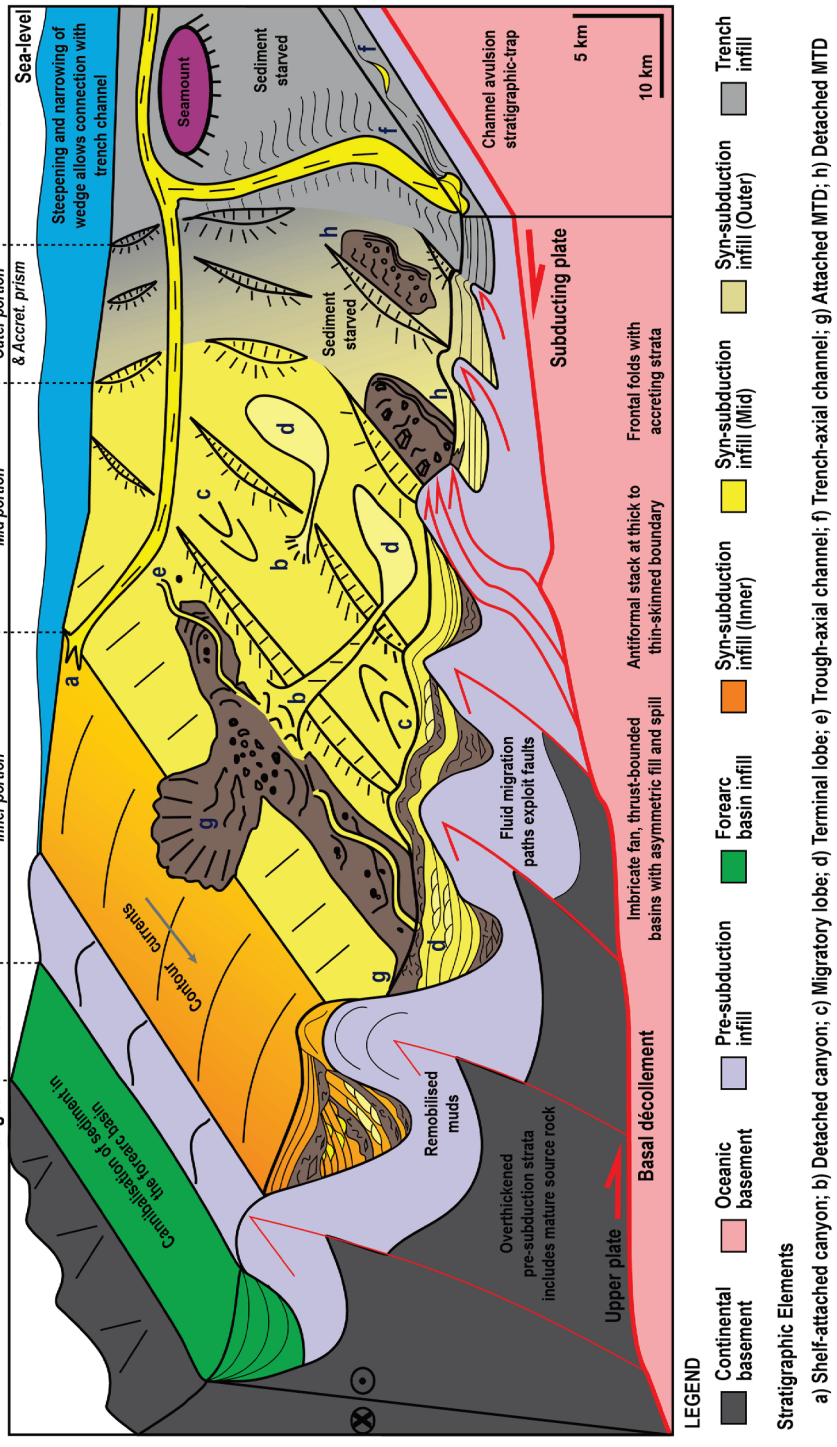

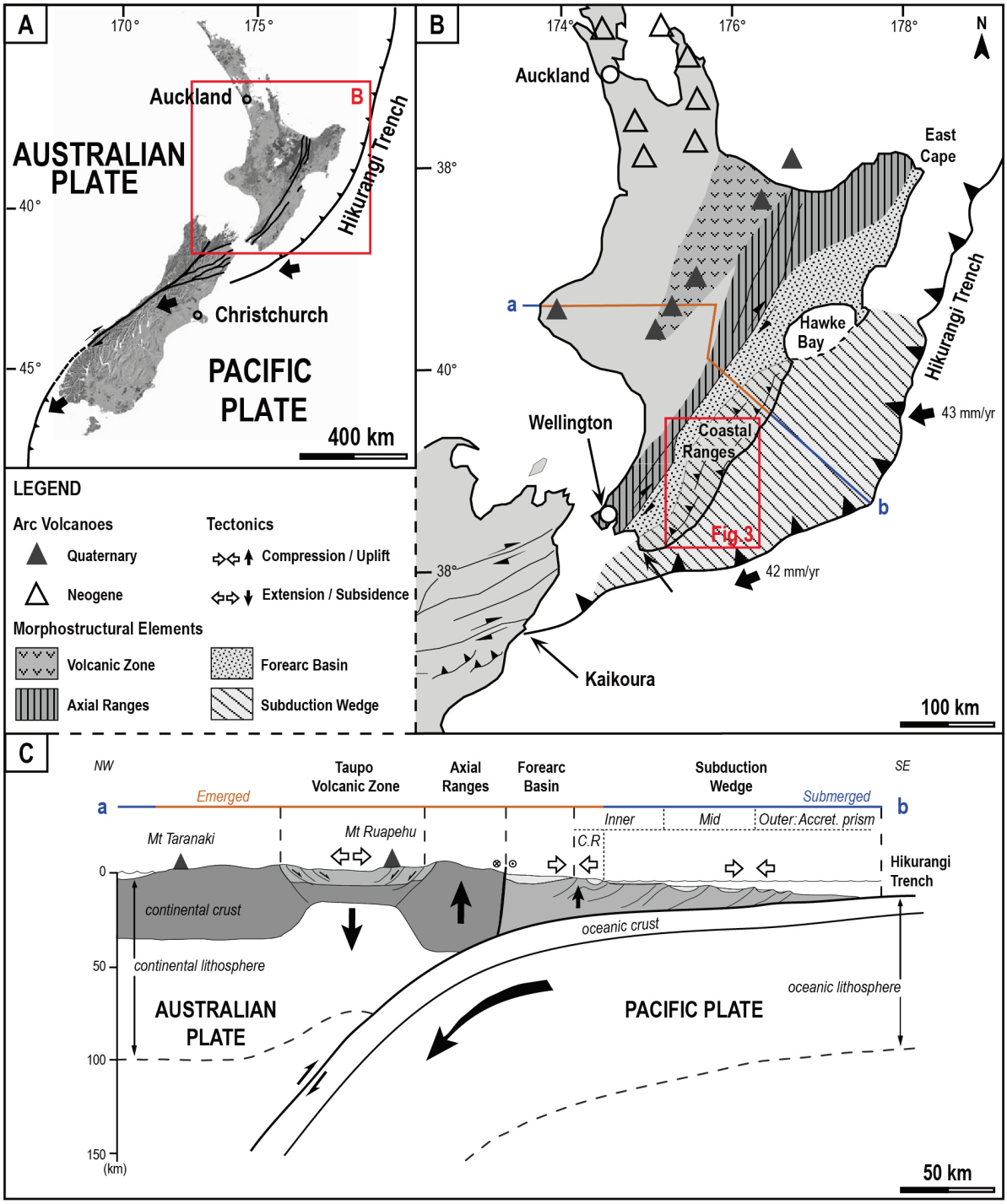

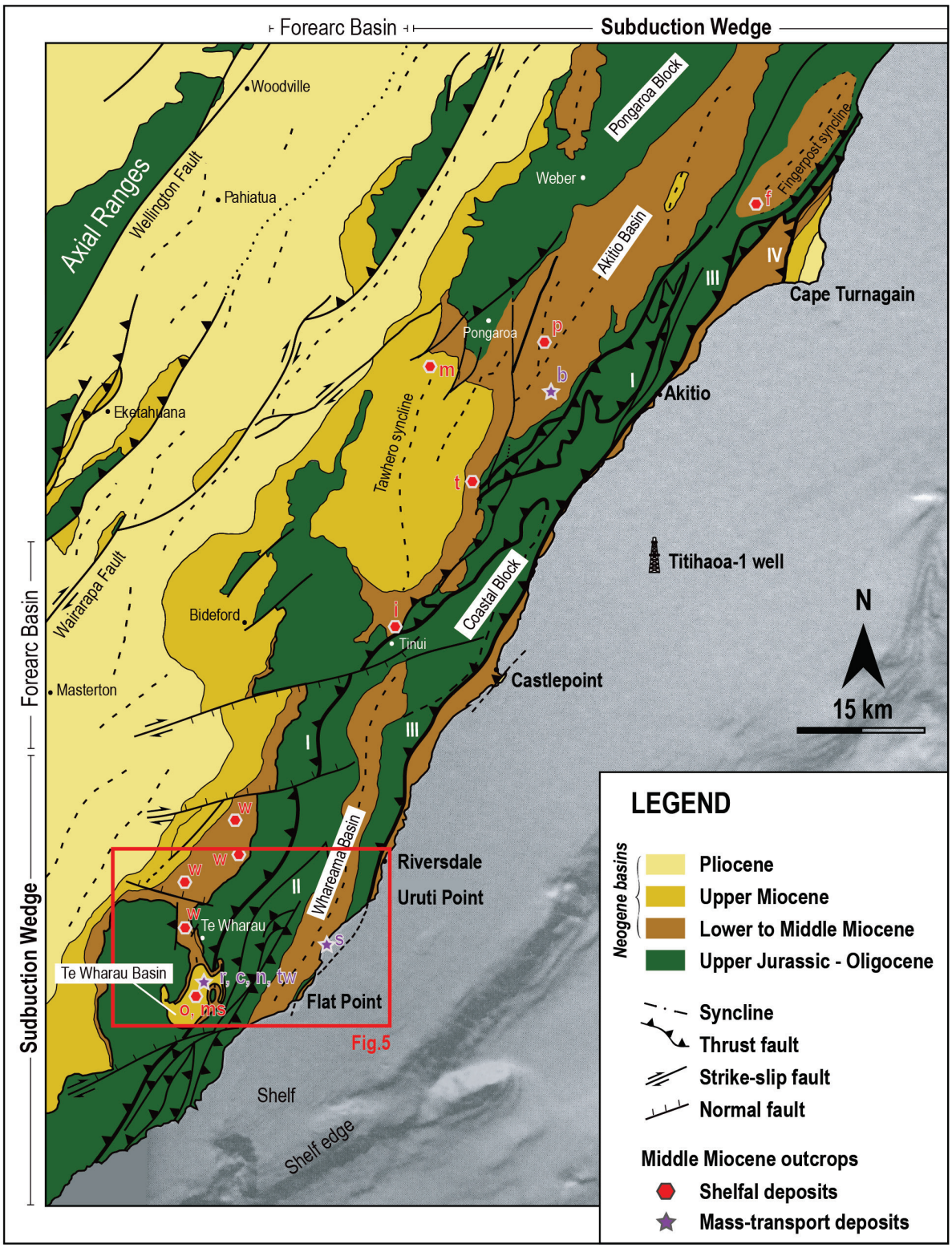

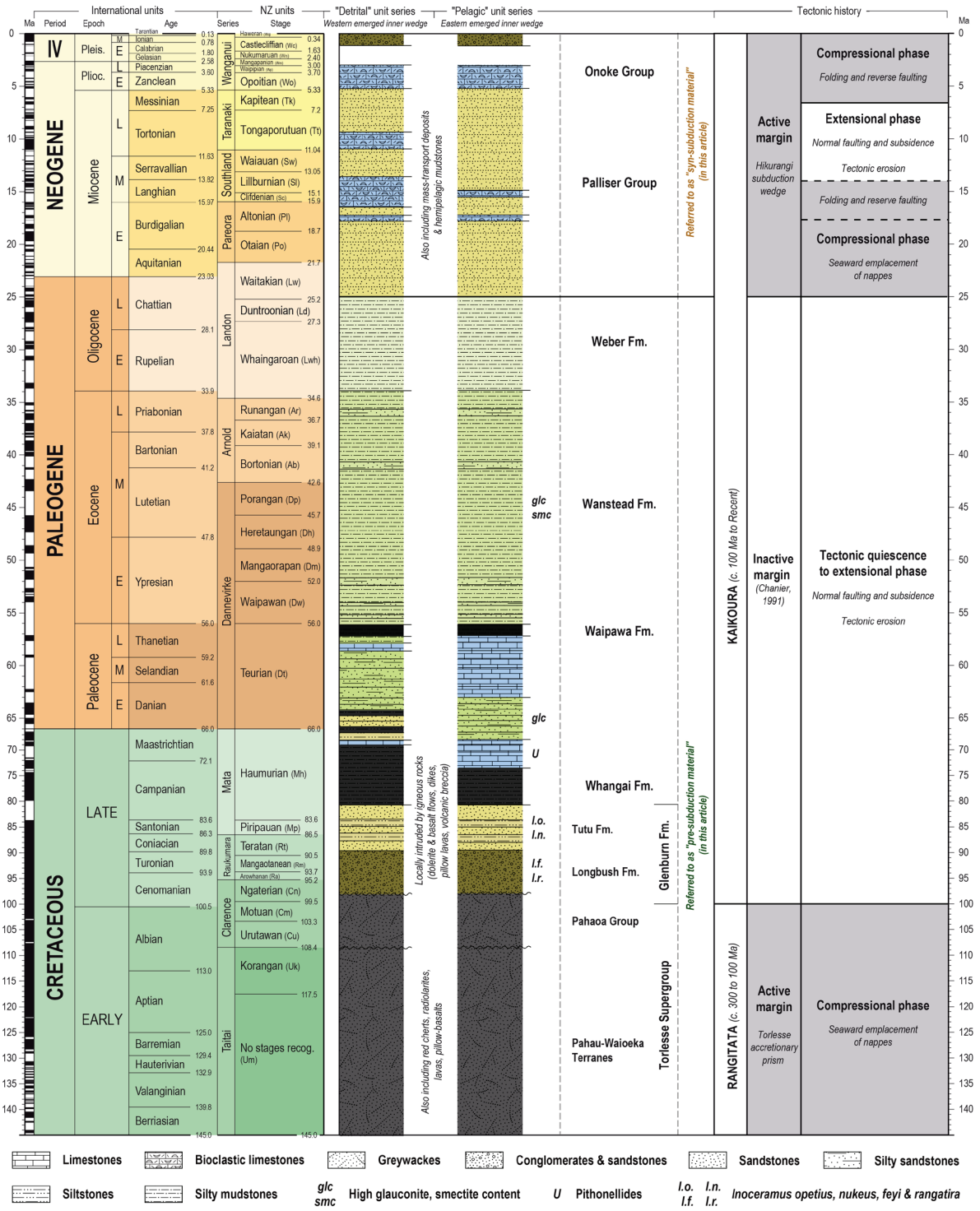
International units
NZ units
"Detrital" unit series
Western emerged inner wedge
"Pelagic" unit series
Eastern emerged inner wedge
Tectonic history
Ma
Period
Epoch
Age
Series
Stage
NEOGENE
PALEOGENE
CRETACEOUS
Pleis.
Plioc.
Miocene
Oligocene
Eocene
Paleocene
LATE
EARLY
Tarantian
Ionian
Calabrian
Gelasian
Piacenzian
Zanclean
Messinian
Tortonian
Serravallian
Langhian
Burdigalian
Aquitanian
Chattian
Rupelian
Priabonian
Bartonian
Lutetian
Ypresian
Thanetian
Selandian
Danian
Maastrichtian
Campanian
Santonian
Coniacian
Turonian
Cenomanian
Albian
Aptian
Barremian
Hauterivian
Valanginian
Berriasian
Wanganui
Taranaki
Southland
Pareora
Landon
Arnold
Dannewirke
Mata
Raukumara
Clarence
Taitai
Castlecliffian (Wc)
Nukumaruan (Wn)
Mangapanian (Wm)
Waipipian (Ww)
Opoitian (Wo)
Kapitean (Tk)
Tongaporutuan (Tt)
Waiauan (Sw)
Lillburnian (Sl)
Clifdenian (Sc)
Altonian (Pl)
Otaian (Po)
Waitakian (Lw)
Duntroonian (Ld)
Whaingaroan (Lwh)
Runangan (Ar)
Kaiatan (Ak)
Bortonian (Ab)
Porangan (Dp)
Heretaungan (Dh)
Mangaorapan (Dm)
Waipawan (Dw)
Teurian (Dt)
Haumurian (Mh)
Piripauan (Mp)
Teratan (Rt)
Mangaotanean (Rm)
Arowhanan (Ra)
Ngaterian (Cn)
Motuan (Cm)
Urutawan (Cu)
Korangan (Uk)
No stages recog. (Um)
Also including mass-transport deposits & hemipelagic mudstones
Locally intruded by igneous rocks (dolerite & basalt flows, dikes, pillow lavas, volcanic breccia)
Also including red cherts, radiolarites, lavas, pillow-basalts
Onoke Group
Palliser Group
Weber Fm.
Wanstead Fm.
Waipawa Fm.
Whangai Fm.
Tutu Fm.
Longbush Fm.
Glenburn Fm.
Pahaoa Group
Pahau-Waioeka Terranes
Torlesse Supergroup
glc
smc
U
l.o.
l.n.
l.f.
l.r.
Referred to as "syn-subduction material" (in this article)
Referred to as "pre-subduction material" (in this article)
KAIKOURA (c. 100 Ma to Recent)
RANGITATA (c. 300 to 100 Ma)
Active margin
Hikurangi subduction wedge
Compressional phase
Folding and reverse faulting
Extensional phase
Normal faulting and subsidence
Tectonic erosion
Folding and reserve faulting
Compressional phase
Seaward emplacement of nappes
Inactive margin (Chanier, 1991)
Tectonic quiescence to extensional phase
Normal faulting and subsidence
Tectonic erosion
Active margin
Torlesse accretionary prism
Compressional phase
Seaward emplacement of nappes
Limestones
Bioclastic limestones
Greywackes
Conglomerates & sandstones
Sandstones
Silty sandstones
Siltstones
Silty mudstones
glc smc High glauconite, smectite content
U Pithonellides
l.o. l.n. l.f. l.r. Inoceramus opetius, nukeus, feyi & rangatira

LEGEND
Neogene basins
Pliocene
Upper Miocene
Lower to Middle Miocene
Upper Cretac. - Oligocene
Lower Cretaceous Torlesse
Syncline
Thrust fault
Strike-slip fault
Middle Miocene outcrops
Shelfal deposits
Mass-transport deposits
N
2 km
Uruti Point
Drone acquisition
s-1
s-2
FLAT POINT FAULT
Flat Point
Whareama Basin
PUKERORO FAULT
GLENBURN FAULT
Glenburn Nappe
TUTU FAULT
ADAMS-TINUI FAULT
Te Wharau
Te Wharau Basin
w-1
w-2
w-3
tw-1
tw-2
ms
c
o
r
n
0

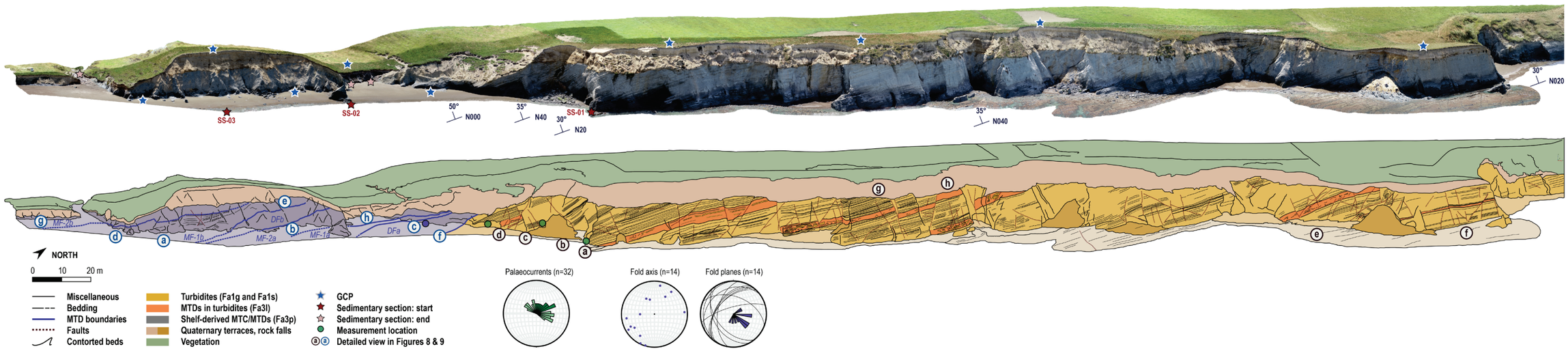
SS-03
SS-02
SS-01
50°
N000
35°
N40
30°
N20
35°
N040
30°
N020
MF-2b
MF-1b
MF-2a
MF-1a
DFb
DFa
NORTH
0 10 20 m
Miscellaneous
Bedding
MTD boundaries
Faults
Contorted beds
Turbidites (Fa1g and Fa1s)
MTDs in turbidites (Fa3l)
Shelf-derived MTC/MTDs (Fa3p)
Quaternary terraces, rock falls
Vegetation
GCP
Sedimentary section: start
Sedimentary section: end
Measurement location
Detailed view in Figures 8 & 9
Palaeocurrents (n=32)
Fold axis (n=14)
Fold planes (n=14)

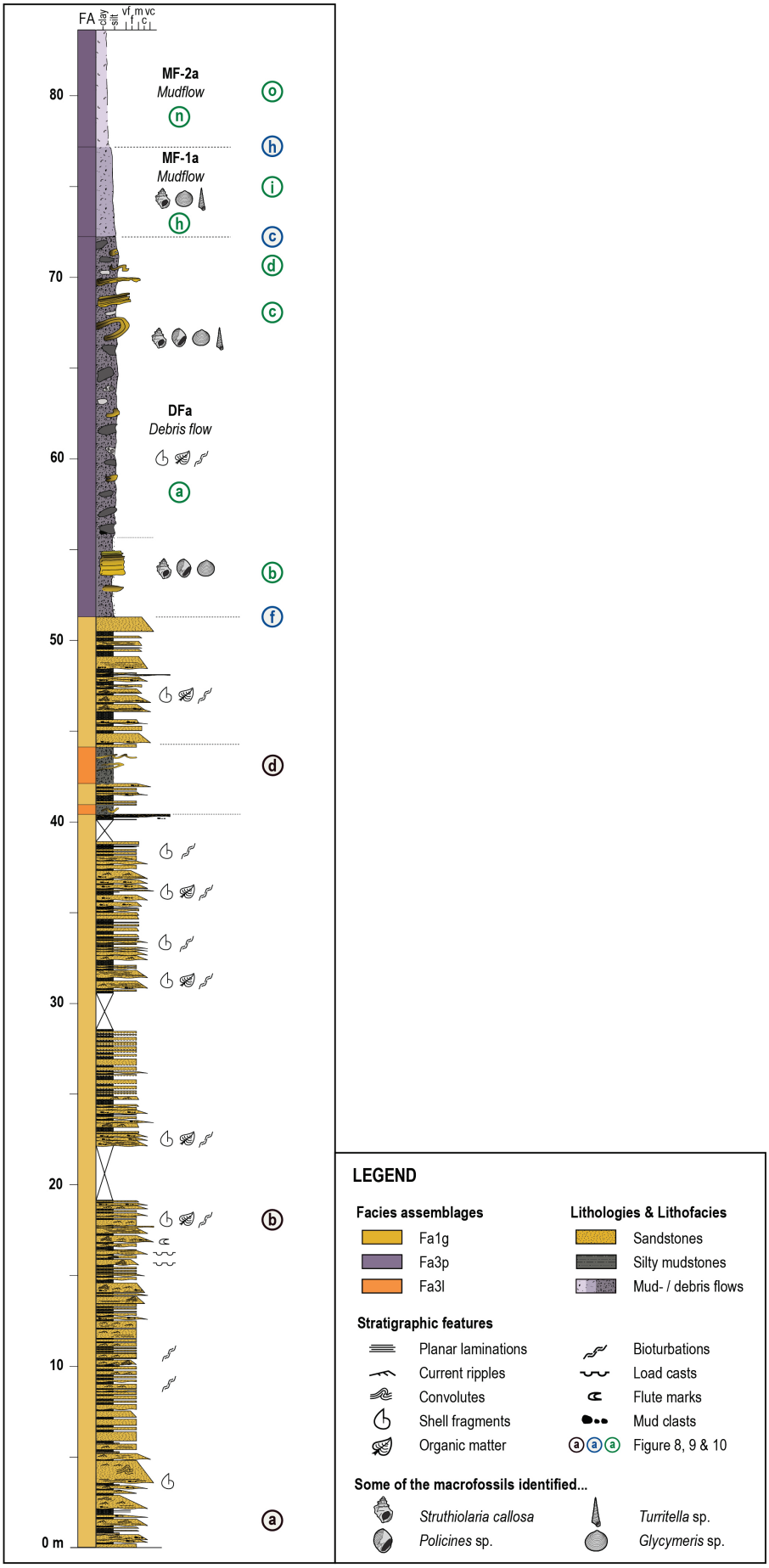

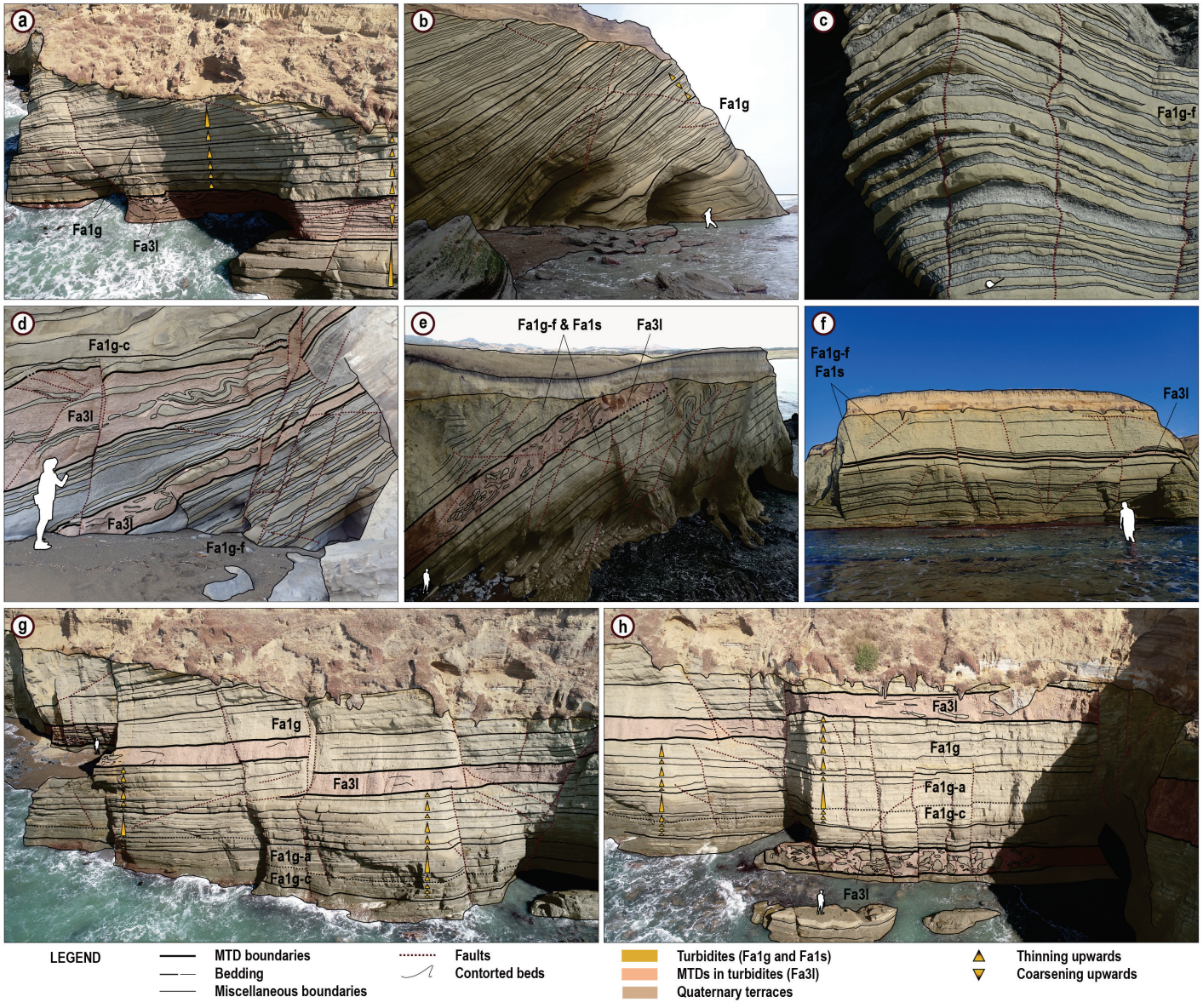

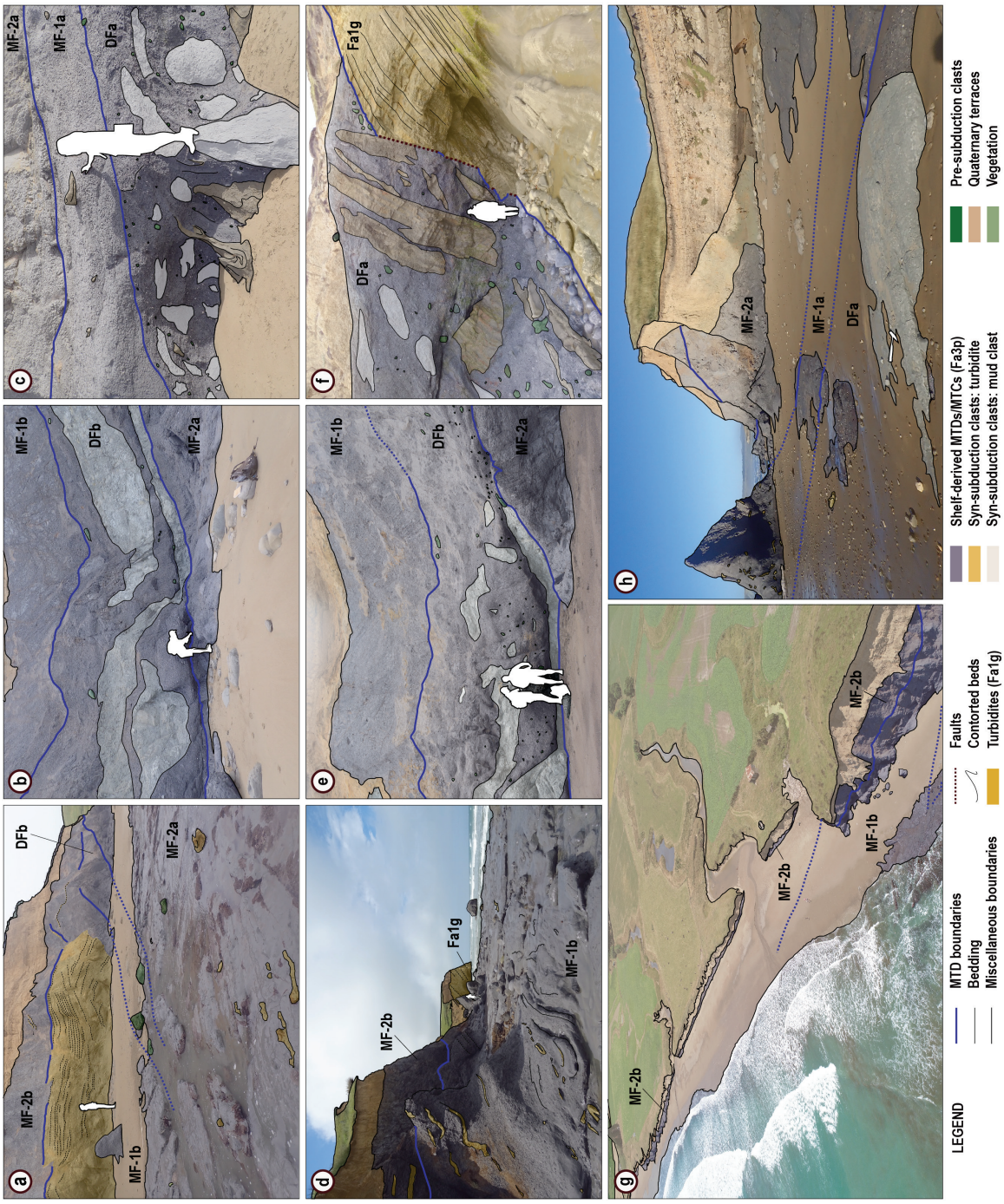
a
MF-2b
DFb
MF-2a
MF-1b
b
MF-1b
DFb
MF-2a
c
MF-2a
MF-1a
DFa
d
MF-2b
Fa1g
MF-1b
e
MF-1b
DFb
MF-2a
f
Fa1g
DFa
g
MF-2b
MF-2b
MF-1b
MF-2b
h
MF-2a
MF-1a
DFa
LEGEND
MTD boundaries
Bedding
Miscellaneous boundaries
Faults
Contorted beds
Turbidites (Fa1g)
Shelf-derived MTDs/MTCs (Fa3p)
Syn-subduction clasts: turbidite
Syn-subduction clasts: mud clast
Pre-subduction clasts
Quaternary terraces
Vegetation

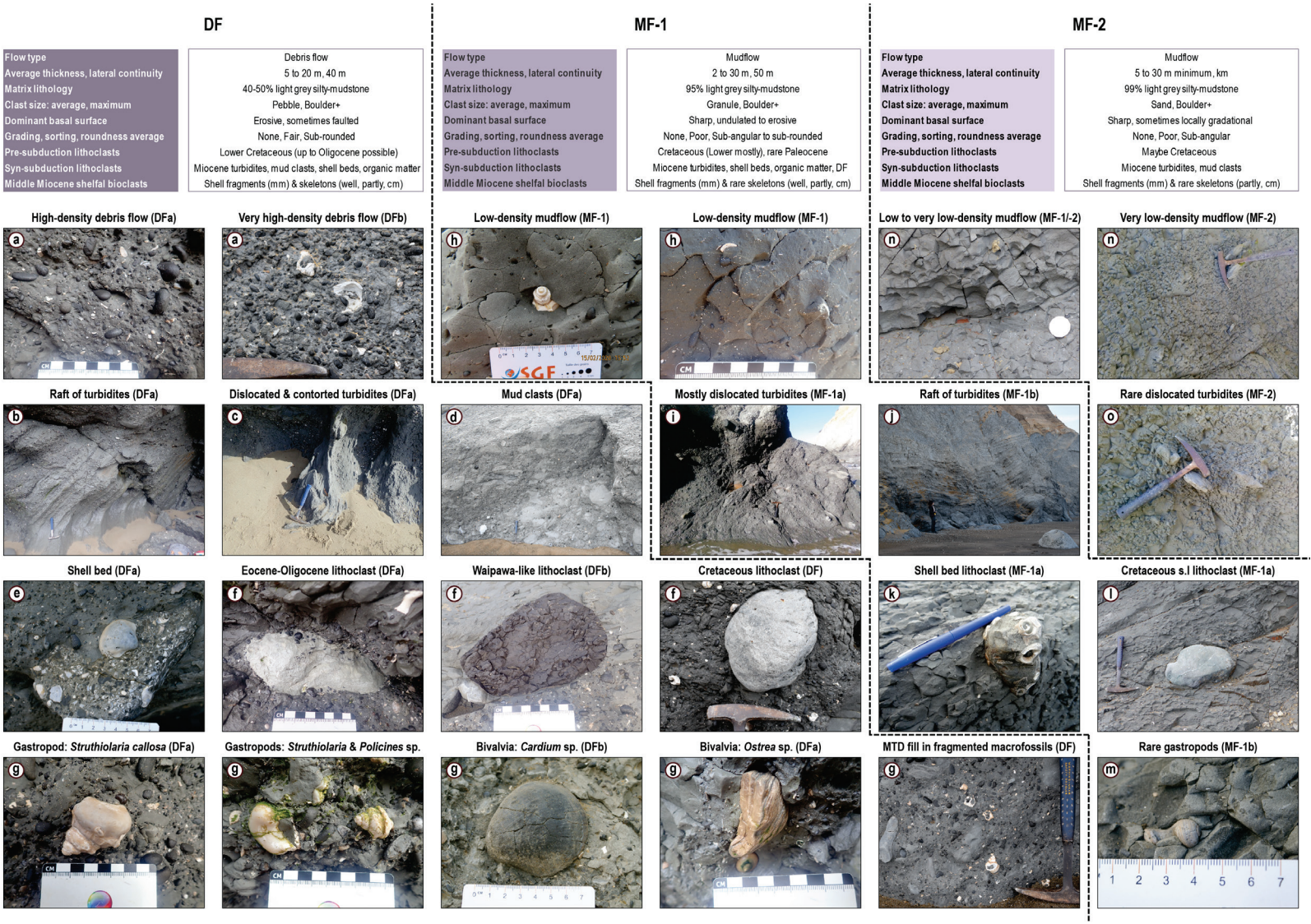

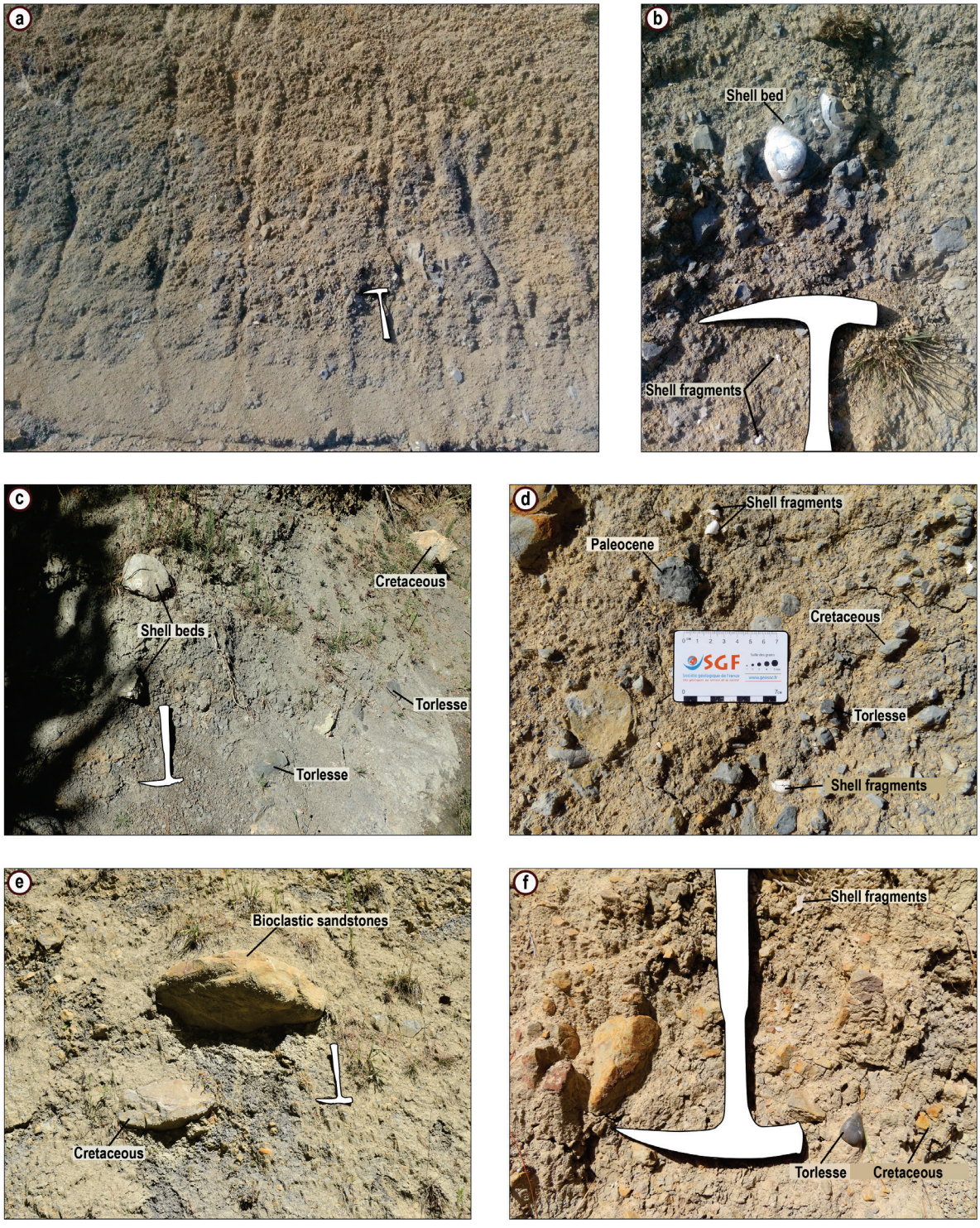
a
b
Shell bed
Shell fragments
c
Cretaceous
Shell beds
Torlesse
Torlesse
d
Shell fragments
Paleocene
Cretaceous
Torlesse
Shell fragments
e
Bioclastic sandstones
Cretaceous
f
Shell fragments
Torlesse
Cretaceous

SEFTON HILLS OUTCROP - SECTION S-1

Bioclastic fraction (0.5 cm-3 cm)

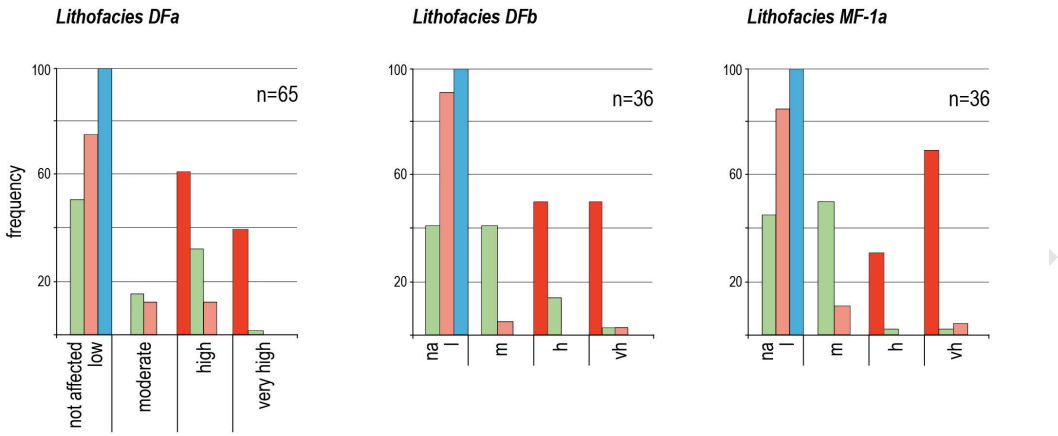

Bioclastic fraction (>3 cm)

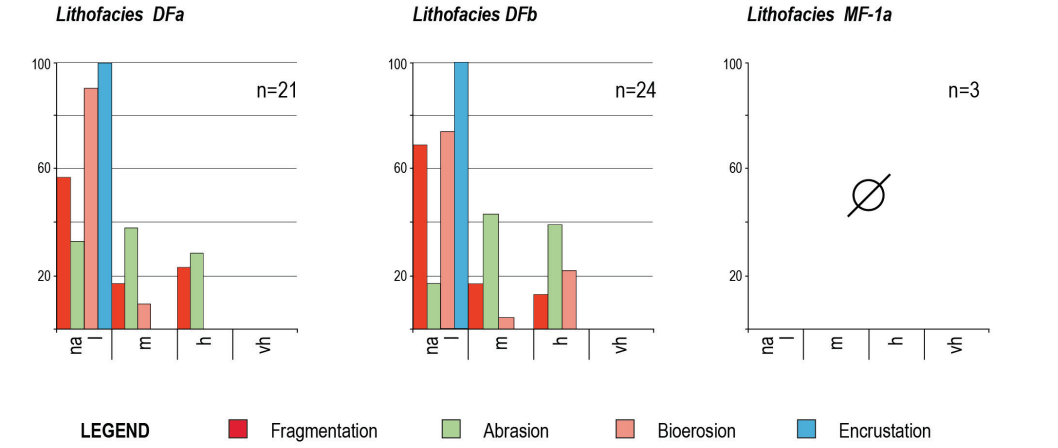

Field photographs showing examples of shell damages

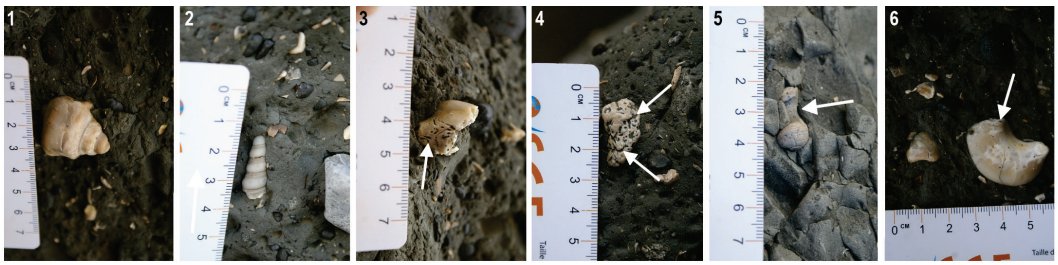

1	2	3	4	5	6
Frag.: Moderate Abr.: High Bioer.: No Encr.: No	Frag.: Moderate Abr.: High Bioer.: No Encr.: No	Frag.: Very High Abr.: Moderate Bioer.: High Encr.: No	Frag.: Very High Abr.: High Bioer.: Very High Encr.: No	Frag.: Very High Abr.: Very High Bioer.: Moderate Encr.: No	Frag.: Very High Abr.: High Bioer.: No Encr.: No

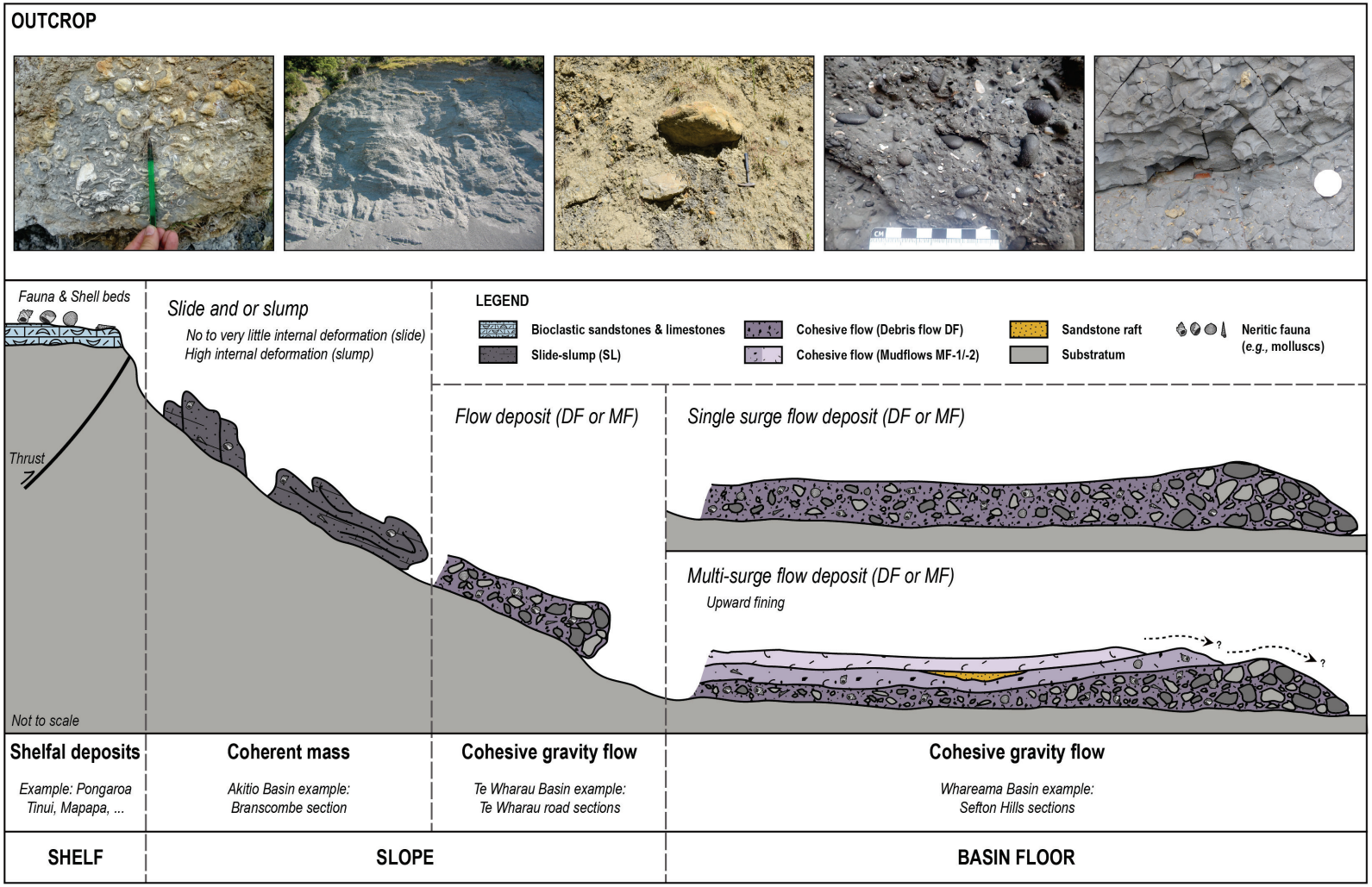

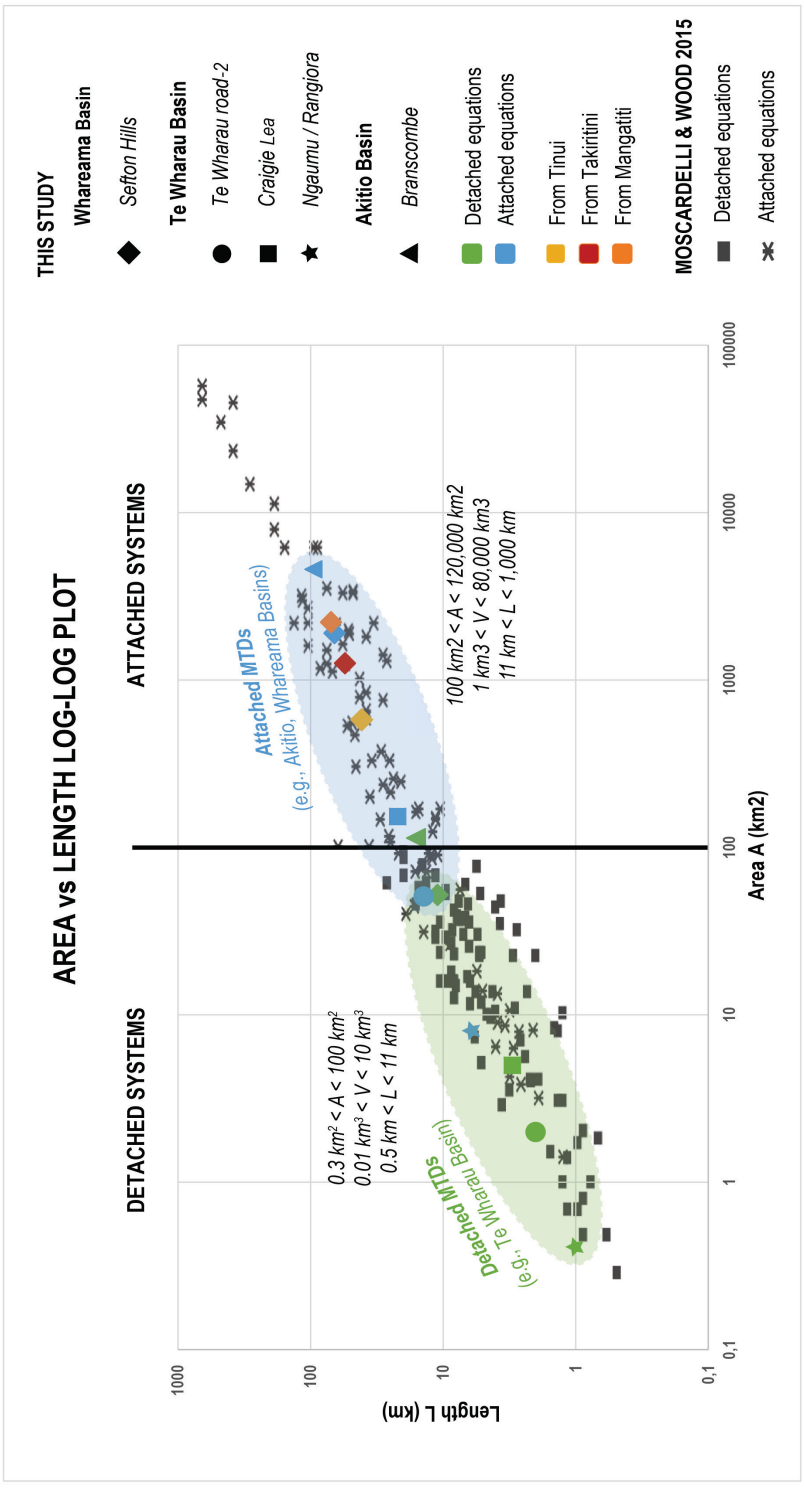
AREA vs LENGTH LOG-LOG PLOT
DETACHED SYSTEMS
ATTACHED SYSTEMS
Length L (km)
Area A (km2)
1000
100
10
1
0,1
0,1
1
10
100
1000
10000
100000
0.3 km² < A < 100 km²
0.01 km³ < V < 10 km³
0.5 km < L < 11 km
100 km2 < A < 120,000 km2
1 km3 < V < 80,000 km3
11 km < L < 1,000 km
Attached MTDs
(e.g., Akitio, Whareama Basins)
Detached MTDs
(e.g., Te Wharau Basin)
THIS STUDY
Whareama Basin
Sefton Hills
Te Wharau Basin
Te Wharau road-2
Craigie Lea
Ngaumu / Rangiora
Akitio Basin
Branscombe
Detached equations
Attached equations
From Tinui
From Takiritini
From Mangatiti
MOSCARDELLI & WOOD 2015
Detached equations
Attached equations

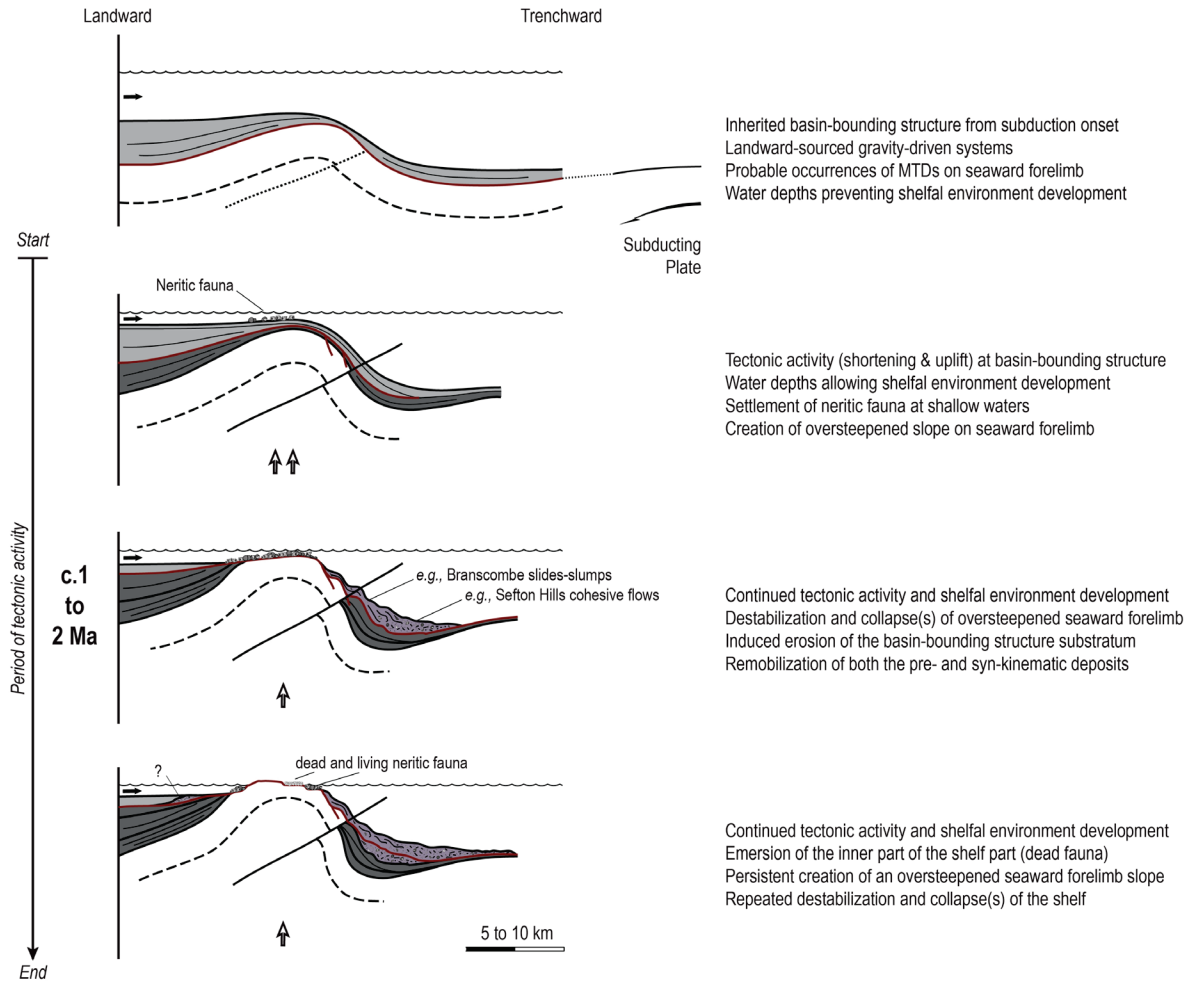
Landward
Trenchward
Subducting Plate
Start
End
Period of tectonic activity
Neritic fauna
c.1 to 2 Ma
e.g., Branscombe slides-slumps
e.g., Sefton Hills cohesive flows
?
dead and living neritic fauna
5 to 10 km
Inherited basin-bounding structure from subduction onset
Landward-sourced gravity-driven systems
Probable occurrences of MTDs on seaward forelimb
Water depths preventing shelfal environment development
Tectonic activity (shortening & uplift) at basin-bounding structure
Water depths allowing shelfal environment development
Settlement of neritic fauna at shallow waters
Creation of oversteepened slope on seaward forelimb
Continued tectonic activity and shelfal environment development
Destabilization and collapse(s) of oversteepened seaward forelimb
Induced erosion of the basin-bounding structure substratum
Remobilization of both the pre- and syn-kinematic deposits
Continued tectonic activity and shelfal environment development
Emersion of the inner part of the shelf part (dead fauna)
Persistent creation of an oversteepened seaward forelimb slope
Repeated destabilization and collapse(s) of the shelf
LEGEND
Syn-subduction, syn-kinematic mass-transport deposits
Syn-subduction, syn-kinematic undiff. gravity-driven deposits
Syn-subduction, pre-kinematic undiff. gravity-driven deposits
Pre-subduction basement
Feeding direction, possible direct continental input
Uplift
Neritic fauna (e.g., molluscs)
Shell fragments

Continental input?
Pongaroa area
Cape Turnagain area
Kings canyon area
Castlepoint area
Tinui area
Towards Flat Point
Wharau area
Continental input?
N
8 km
LEGEND
Land
Shelfal environments
Shelf-derived mass-transport systems
Turbidite system
Trench-slope basin slope and floor
Feeding direction
Middle Miocene (SI) outcrops
Shelfal deposits (southern & northern)
Mass-transport deposits (from distinct shelves)

System code	Fa code	LF code	Lithology	Stratification	Internal bedding	Interpretations	Depositional environment
Fa1 **Turbidite systems** Alternation of sandstones, siltstones and mudstones	Fa1g - Depositional lobe	Fa1g-c	LF2 (Burgreen and Graham, 2014; McArthur et al., 2020); Fa1g (Bailleul et al., 2007)	Fine- to coarse-grained sandstones and silstones, well-sorted, with mudstone cap.	Thin- to thick-bedded sandstones, thickness varies laterally but remains relatively continuous, irregular incisional base with cm to dcm scale incisions truncating underlying strata sometimes with channel-based drapes (CBDs), gradational to sharp tops.	Medium to coarse-grained Ta in thicker beds, commonly massive / structureless, with mud clasts, shell and plant fragments, sometimes displaying sole marks such as flute casts. Planar laminations (Tb), often dewatering or soft sedimentation deformation structures above well-developed climbing ripples (Tc). Lamination often highlighted by organic rich, carbonaceous and shell fragments. Common amalgamation and some aggradational successions. Rare bioturbation in mudstone cap. Possible stack of several set-scale cycles with intrachannel mudstones.	High sedimentation rate with rapid suspension fall-out from high density, mostly erosive turbidity currents (Lowe, 1982; Kneller, 1995). Small-scale incisional features suggesting small erosional channels and discontinuous scours developing on the surface of a lobe (Burgreen and Graham, 2014). CBDs resulting from abandonment after initial incison or developing progressively as the channel fills (Barton et al., 2010). Fragment content suggests that flow initiated in shallow marine environment.	Distributary channels and scours. Lobe off-axis, proximal to medial region.
		Fa1g-a	LF2 (Burgreen and Graham, 2014); Fa1g (Bailleul et al., 2007)	Very fine- to medium-grained sandstones and silstones, well-sorted, with mudstone cap.	Thin- to medium-bedded sandstones, fining and thinning upwards alternation, good lateral continuity yet pinches out, sharp or slightly irregular bases and gradational to sharp tops.	Rare basal coarse Ta intervals, occasional planar laminations (Tb) passing into climbing ripples (Tc), mostly climbing ripples passing into massive (due to bioturbation?) / structureless facies. Lamination often highlighted by organic rich, carbonaceous and shell fragments. Rare amalgamation. Very common bioturbation in mudstone cap.	Slow deposition from a mostly non-erosive, waning, high- to low-density turbidity currents (Lowe, 1982; Kneller, 1995). Fragment content suggests that flow initiated in shallow marine environment. Upward fining and thinning suggest abandonment of the channel and filling of the unfilled reflief (McHargue et al., 2011).	Abandonment / Spill of distributary channels. Lobe off-axis, proximal to medial region.
		Fa1g-f	LF1 (Burgreen and Graham, 2014); LF4, LF5, LF6 or LA2 (McArthur et al., 2020); Fa1g (Bailleul et al., 2007)	Very fine- to fine-grained sandstones and silstones, well-sorted, with bioturbated mudstone cap.	Very thin- to medium-bedded sandstones, thinning or thickening upwards, lateral continuity yet pinching out possible, mostly slightly irregular bases and gradational to sharp tops, local low-displacement slumps and slump scours (Fa3l-s).	Mostly wheathered or bioturbated, occasional planar laminations (Tb) passing into climbing ripples (starved) and rare convolutes (Tc). Sometimes alternation of parallel- and ripple-laminated sandstone to siltstone. Rare incisional features with coarser material and occasional bioclastic grits. Lamination often highlighted by organic rich, carbonaceous and shell fragments. Variable degree of bioturbation, tends to be highly bioturbated.	High sedimentation rate with deposition from a mostly non-erosive, waning, low-density turbidity currents (Lowe, 1982; Kneller, 1995). Alternation of waxing then waning flow possibly indicating hyperpycnal flows (Mulder et al., 2003). Fragment content suggests that flow initiated in shallow marine environment.	Lobe fringe, medial to distal region.
	Fa1s - Sheet-like	Fa1s	Fa1s (Bailleul et al., 2007)	Mostly fine-grained sandstones and siltstones, well-sorted, with bioturbated mudstone cap.	Thin- to very thick-bedded, tabular (sheets), good lateral continuity, sharp erosional bases and gradational to sharp tops, local low-displacement slumps and slump scours (Fa3l-s).	Commonly massive, sometimes planar laminations (Tb), rare ripples and convolutions (Tc), intra-beds erosional to non-erosional amalgamation surfaces. Lamination can be highlighted by organic rich, carbonaceous and shell fragments. Mostly a sandy succession.	Unconfined turbidity currents. Deposition from waning, low density turbidity currents (Lowe, 1982; Kneller, 1995).	Sheet-lobe, distal region. Sheet-like turbidites.
Fa3 **Mass-wasting systems** Disorganized gravels, sandstones, siltstones and mudstones	Fa3l - Locally-derived	Fa3l-d	LF6 (Burgreen and Graham, 2014)	Matrix-supported, siltstones to silty mudstones with varying quantity of granule- to boulder-grade syn-subduction extraformational clasts.	Sharp and planar base and sharp sometimes undulated top, laterally continuous with sometimes the undeformed interval laterally available and visible, usually between 1 to 5 m thick interval.	Ungraded, disorganized. Syn-subduction lithoclasts (sandstone to siltstone). Rare syn-subduction bioclasts. Possible recumbent folds, shear and load structures.	Cohesive flow: debris flow or mudflow (Nardin et al., 1979; Mulder & Alexander, 2001). Possible flow transformation of Fa3l-s. Located within a deep-marine turbidite system thereby suggesting a local destabilization. Punctual bioclastic material could result from storms.	Locally-sourced mass-transport deposits.
		Fa3l-s	LF6 (Burgreen and Graham, 2014)	Disorganized interbedded sandstones, siltstones and mudstones. Silty mudstone background facies with occasional granule- to boulder-grade intraformational clasts.	Sharp and planar base and sharp sometimes undulated top, laterally continuous with sometimes the undeformed interval laterally available and visible, usually between 1 to 5 m thick interval.	Contorted (recumbent folds), remobilized. Possible scattered, syn-subduction lithoclasts (dislocated turbidites). Syn-sedimentary deformation.	Coherent mass of sediment that moves along a glide plane (Nardin et al., 1979), either resulting in no, very little or significant internal deformation. Slide or slump (function of basal shearing surface). Located within turbidite system thereby suggesting local destabilization.	
	Fa3p - Shelf-derived	Fa3p-d	DF, MF-1, MF-2	Matrix-supported, siltstones to silty mudstones with varying quantity of granule- to boulder-grade pre- and syn-subduction extraformational clasts.	Slightly to highly erosive base and sharp to undulated top, sometimes gradational top, laterally discontinuous, variable thickness (m to dm).	Ungraded, disorganized. Pre- and syn-subduction lithoclasts. Syn-subduction bioclasts, either as skeletons (gastropods, bivalvia, corals) and or shell fragments. Common recumbent folds, shear and load structures.	Cohesive flow: debris flow or mudflow (Nardin et al., 1979; Mulder & Alexander, 2001). Macrofaunal assemblages suggest that mass-wasting initiated in shallow marine environment.	Shelf-derived mass-transport deposits.
		Fa3p-s	SL	(Dis)organized interbedded sandstones, siltstones and mudstones. Sandy to silty mudstone background facies with granule- to boulder-grade pre- and syn-subduction extraformational clasts (litho- & bioclasts).	Sharp and planar base and sharp sometimes undulated top, laterally continuous with sometimes the undeformed interval laterally available and visible, usually 10s of m thick intervals.	Coherent to contorted (recumbent folds), remobilized. Pre- and syn-subduction lithoclasts. Syn-subduction bioclasts, either as skeletons (gastropods, bivalvia, corals) and or shell fragments. Syn-sedimentary deformation.	Coherent mass of sediments that moves along a glide plane (Nardin et al., 1979), either resulting in no, very little or significant internal deformation. Slide or slump (function of basal shearing surface). Macrofaunal assemblages suggest that mass-wasting initiated in shallow marine environment.	